A Geospatial Approach for Analysis of Drought Impacts on Vegetation Cover and Land Surface Temperature in the Kurdistan Region of Iraq

Heman Abdulkhaleq A. Gaznayee [1,*] , Ayad M. Fadhil Al-Quraishi [2,*] , Karrar Mahdi [3] and Coen Ritsema [3]

1 Department of Forestry, College of Agriculture Engineering Science, Salahaddin University, Erbil 44003, Kurdistan Region, Iraq
2 Petroleum and Mining Engineering Department, Faculty of Engineering, Tishk International University, Erbil 44001, Kurdistan Region, Iraq
3 Soil Physics and Land Management Group, Wageningen University & Research, 6700 AA Wageningen, The Netherlands; karrar.mahdi@wur.nl (K.M.); coen.ritsema@wur.nl (C.R.)
* Correspondence: heman.ahmed@su.edu.krd (H.A.A.G.); ayad.alquraishi@tiu.edu.iq (A.M.F.A.-Q.)

Abstract: Drought is a common event in Iraq's climate, and the country has severely suffered from drought episodes in the last two decades. The Kurdistan Region of Iraq (KRI) is geographically situated in the semi-arid zone in Iraq, whose water resources have been limited in the last decades and mostly shared with other neighboring countries. To analyze drought impacts on the vegetation cover and the land surface temperature in the KRI for a span of 20 years from 1998 to 2017, remote sensing (RS) and Geographical Information Systems (GIS) have been adopted in this study. For this study, 120 Landsat satellite images were downloaded and utilized, whereas six images covering the entire study area were used for each year of the study period. The Normalized Difference Vegetation Index (NDVI) and Land Surfaces Temperature Index (LST) were applied to produce multi-temporal classified drought maps. Changes in the area and values of the classified NDVI and LST were calculated and mapped. Mann–Kendall and Sen's Slope statistical tests were used to assess the variability of drought indices variation in 60 locations in the study area. The results revealed increases in severity and frequency of drought over the study period, particularly in the years 2000 and 2008, which were characterized by an increase in land surface temperatures, a decrease in vegetation area cover, and a lack of precipitation averages. Climate conditions affect the increase/decrease of the vegetated cover area, and geographical variability is also one factor that significantly influences the distribution of vegetation. It can be concluded that the southeast and southwestern parts of the KRI were subjected to the most severe droughts over the past 20 years.

Keywords: drought; KRI; NDVI; LST

1. Introduction

Among all natural disasters, drought can be considered the most complex due to the difficulties in identifying its start, end, intensity, and extent [1]. Droughts cause enormous sufferings for the society and the environment. Consequently, it is important to learn drought's spatial-temporal pattern [2]. Several environmental factors play significant roles in the occurrence of droughts, high temperature and winds, relatively low humidity, timing, characteristics, and patterns of rains—especially during crop growing seasons, intensity and duration of rainfall, and onset and termination [3]. Although drought has no universal definition, it can be simply defined as the deficit in precipitation and terrestrial water storage (the sum of surface and subsurface water), which adversely impacts agriculture, the environment, and the economy [4,5]. Drought has a significant adverse impact on the socio-economic, agricultural, and environmental sectors [2]. During drought periods, severe water stress can occur in a region due to lack of precipitation, water resources

overexploitation, high rates of evapotranspiration, and/or an amalgamation of those factors [6,7].

Remote sensing plays a vital role in detecting, mapping, assessing, and monitoring the earth's resources and natural hazards at spatiotemporal scales [2]. Various techniques and indices have been developed to address and manage drought status. The leading cause of drought is the lack of rainfall averages below normal levels; however, human and social activities also lead to drought [7,8]. The occurrence of high temperatures and low moisture levels is often related to drought events, which have become quite frequent in recent years; thus, it is predominantly associated with climate change [9]. The influence of drought might also vary geographically due to variability in precipitation patterns and human resilience [7]. The National Oceanic and Atmospheric Administration (NOAA) has defined the drought background and its effect on Iraqi lands as the decline in rainfall averages for long periods, for a season or more, which leads to water stress-causing negative effects on the water resources and consequently adverse impacts on the plants, animals, and people [10]. In the series of drought development, there are two phases. The first is the meteorological drought that occurs when there is an extended decrease in rainfall rates compared to the normal rates. Secondly, the lack of rainfall is one reason that leads to a decrease in soil moisture. Thus, the lack of suitable conditions for plant growth and the dwindling of vegetation cover is called agricultural drought [11]. The drought situation in Iraq has been stated by several researchers [12]. In recent years, the annual precipitation averages have been declining due to global warming [13]. The Iraqi report 2009 issued by the Coordination of Humanitarian Affairs, UNAMI, and IAU office, considered the most important reasons for the successive droughts events in Iraq are the decrease in rainfall rates and the water discharge rates decline of the main rivers in Iraq. Consequently, these lead to reduced groundwater levels, the river flows, and draining water sources (springs, deep, and shallow wells) [14]. On the other side, in a span of ten years, from 2003 to 2012, Iraq has suffered several severe droughts, which were results from different reasons, such as low average precipitations, higher temperatures rates, lower water income from the upstream countries, and low efficiency in water utilization [15,16].

Iraq's location in arid and semi-arid regions led to a high frequency of droughts, especially during the last two decades [17]. Low precipitation and its fluctuation during the season are normal in most North African and West Asian countries. This puts Iraq, among other countries, in a place where serious actions on drought management must be adopted [18]. Moreover, in 1999 a severe drought occurred in Erbil and Dohuk, where it also suffered from moderate drought in 1986–1987, 1989–1991, 1999, and 2008 [11,19]. The annual precipitation average in the KRI ranges is from less than 100 mm in the south to 1200 mm in the northeastern mountainous region [14]. From 1999 to 2002, Erbil suffered from a decrease in rainfall averages and drought suffering. It also went through another drought period in 2007–2011, indicating that Erbil is an area prone to drought [20]. Moreover, Sulaymaniyah was subjected to severe droughts from 1994 to 1998 [20,21]. On the other hand, precipitations were significantly decreased in 2008, then a drought took place in the governorate, and similar observations are also noted in the Duhok governorate [12].

Although a few methods were developed in remote sensing for drought monitoring, some others further considered the influence of drought on vegetation. The Normalized Difference Vegetation Index (NDVI) is one of the earliest vegetation indices used to monitor drought; it has been used since the 1980s [18,22,23]. Different studies have been conducted to explore spatiotemporal patterns of drought; however, most of those studies focused on the methods of drought detecting and evaluating the agricultural drought's relationships with each rainfall average and the crop yield using the Landsat time-series dataset [18].

In Iraq, including the Kurdistan region, drought is a common event causing significant agro-economic losses, but there is a significant lack of detailed information on the spatiotemporal patterns of drought severity in the KRI, for which it can be employed to take extra precautions for mitigating its negative impacts [20,21]. Therefore, a detailed analysis of seasonal drought dynamics is required to identify spatiotemporal drought patterns at a

meteorological scale and vegetative spheres [24]. Time-series patterns of droughts in the KRI have been mapped using remote sensing (RS) and Geographic Information Systems (GIS) using various drought indices. Since aquifer recharge, agricultural activities, and ecological changes are affected by rainfall, the focus was on drought during the agriculture growing season [25].

The NDVI, the land surface temperature (LST), and the LST/NDVI slope can have an essential role in monitoring drought, low rainfall, and tracking crop growth, crop yields, weather impact, and the environmental and economic effects [26]. For vegetated regions, the fluctuation in weather-related NDVI cannot be detected easily, as the integrated area of the weather component is smaller than the ecosystem component [7,27]. Hence, it is advised to separate weather components from an ecosystem component when using NDVI to analyze weather's impact on vegetation [28]. Drought analysis requires both drought-causative and responsive parameters, such as rainfall, soil moisture, potential evapotranspiration, vegetation condition, groundwater, and surface water levels. Since drought measuring parameters are not linearly correlated, the correlation among drought indices is usually weak, and typically, they are not predicting similar patterns [29,30].

Using NDVI data, the changes in vegetation cover in the study area were presented, and the trend in drought occurrences can be studied. The NDVI performance is not without errors, such as errors during the growing season and saturation effect on dense vegetation [31]. Therefore, the results have to be validated using other parameters to increase the accuracy [32]. The LST is a good index of the earth's surface's energy balance, providing important information about the surface's physical properties and climate [28]. It was found that there is a negative correlation between LST and NDVI, reported by [31], as an increase of LST was observed at several scales due to changes in vegetation cover and soil moisture, which indicates that the surface temperature can rise rapidly with water stress. Thus, the ratio of LST/NDVI increases during times of drought [31].

This study aims to analyze a spatial pattern for drought severity in the KRI to investigate the spatiotemporal drought characteristics to focus on the agricultural drought assessment by analyzing vegetation stress caused by the lower precipitation. Overall, there are two reasons for selecting the KRI as the research area. First, KRI is prone to drought because of its geographical location and climate. Thus, mastering the mapping and classification of drought characteristics is conducive to forecasting drought in the future. Second, the abovementioned three areas in KRI vary significantly in terms of their topography, NDVI, LST, and precipitation distribution, and thus, the drought characteristics differ considerably among those three areas using Landsat time-series image-based NDVI and LST indices for a span of twenty years from 1998 to 2017.

2. Materials and Methods

2.1. Study Area

The KRI territories were selected as the study area in this research, particularly in Erbil, Sulaimaniyah, and Duhok governorates. The study area is located in the northern part of Iraq. Syria borders the study area from the west, Iran from the east, and Turkey from the north [25]. The KRI is characterized by a Mediterranean climate, which is cold and rainy in winter and hot and dry in summer [33]. It is situated between latitudes 34° and 37° and longitudes 41° and 46°, covering an extent of about 53,000 km², which constitutes a large portion of the entire Iraq territory [34]. It has a diverse physical environment, whereas the elevation ranges from 88 m in its southern parts to more than 3603 m in the north and northeast parts (Figures 1 and 2).

KRI's climate is characterized by high precipitation rates in the northern and mountainous parts, while dry weather is governed in the plains in the southern parts [35]. In general, the precipitation starts from October to May, with 350 mm in the southwestern parts to more than 1200 mm in northern and northeastern parts [36]. Figure 1B and Table 1 explain the data collected from 60 meteorological stations for three different zones in the KRI: assured rainfall zone (>500 mm), semi-assured rainfall zone (350–500 mm), and unas-

sured rainfall zone (<350 mm) [20]. The rain-fed lands represent approximately 37.2% of the total agricultural lands in the KRI [19]. The mean daily temperature varies from 5 °C in winter to 30 °C in summer; however, this rises to 50 °C in the region's southern parts [35]. The total area of forests and pastures in the KRI is 6486.9 and 8397.2 km², respectively, distributed as follows: Erbil 29%, Duhok 28.7%, and Sulaimaniyah 42.3% [25,37].
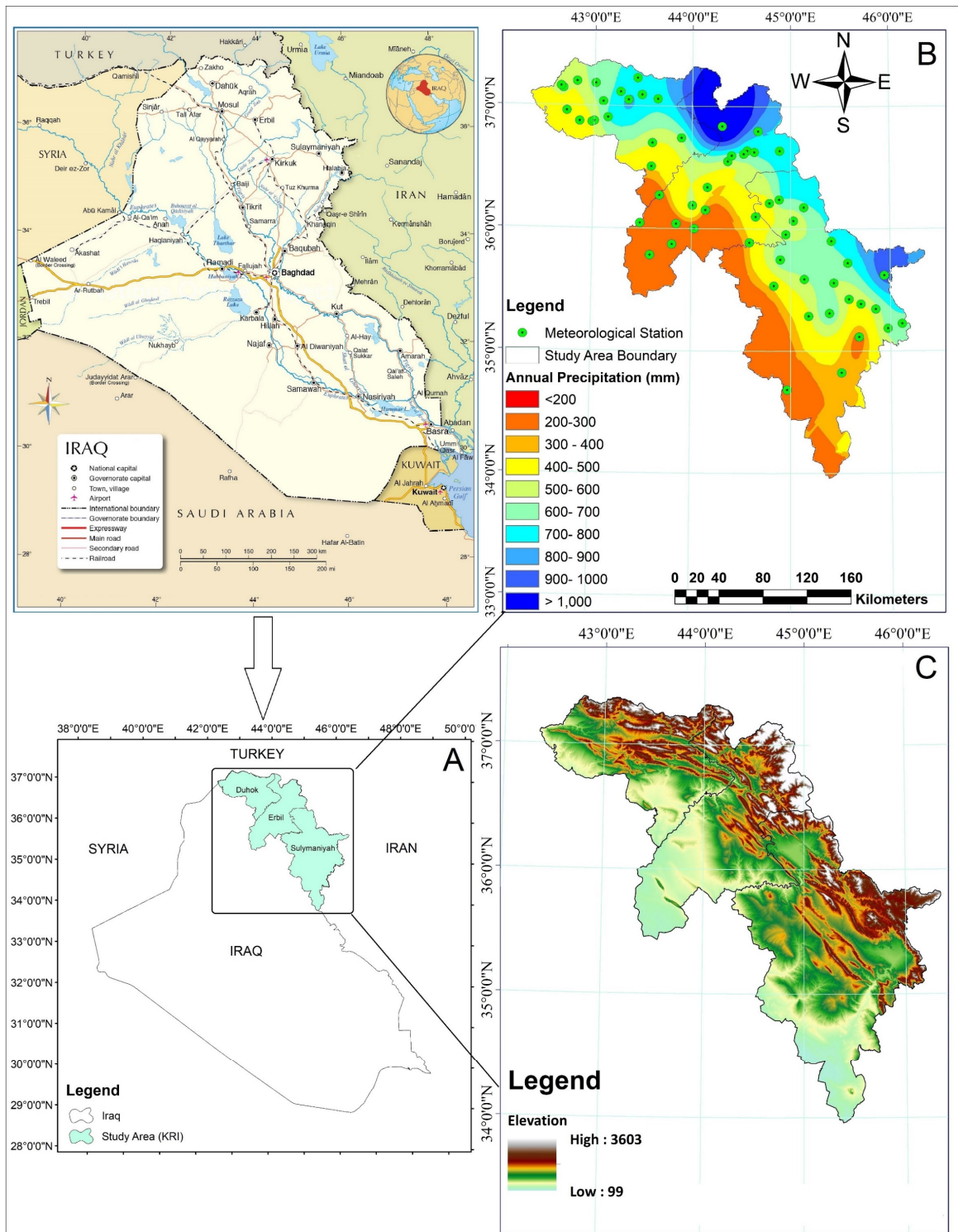
Figure 1. (**A**) Location map of the study area (**B**); The meteorological stations map and the spatial distribution of annual rainfall (mm/year) in the KRI in 1998–2017 (**C**); Digital Elevation Model (DEM).

Table 1. The (AP) annual precipitation (mm), elevation, and coordinates of the 60 (MT) meteorological stations in the KRI used in this study.

MT No.	Station Name	Lat	Long	DEM (m)	AP (mm)	MT No.	Station Name	Lat	Long	DEM (m)	AP (mm)
1	(ER)	36.19111	44.00917	412.7	326.2	31	Mangish	37.03513	43.09252	1030.2	645.0
2	Qushtapa	36.00085	44.02848	390.8	280.6	32	Deraluke	37.05859	43.64925	706.8	759.5
3	Khabat	36.27278	43.67389	285.9	290.9	33	Akre	36.74139	43.89333	683.1	600.0
4	Bnaslawa	36.1538	44.13999	540.7	320.2	34	Amadia	37.0925	43.48722	1148.5	745.7
5	Harir	36.5511	44.3648	837.3	552.2	35	Sarsink	37.05028	43.35028	957.1	841.6
6	Soran	36.63846	44.56136	701.6	625.7	36	Bamarni	37.11512	43.2693	1203.0	722.3
7	Shaqlawa	36.19111	44.00917	966.5	750.0	37	Barda	36.50822	43.58941	363.6	391.4
8	Khalifan	36.5986	44.4038	697.1	670.8	38	Qasrok	36.7009	43.59795	414.8	500.5
9	Choman	36.6374	44.8893	1178.4	732.2	39	(SU)	35.55722	45.43556	870.8	595.0
10	Sidakan	36.79736	44.6714	1011.3	822.5	40	Bazian	35.58902	45.13952	943.7	596.1
11	Rwanduz	36.61194	44.52472	801.6	712.3	41	Halabja	35.18639	45.97389	716.6	648.8
12	Mergasur	36.8382	44.3062	1108.9	1356.0	42	Penjwen	35.61972	45.94139	1442.9	968.7
13	Dibaga	35.87303	43.80496	328.3	246.2	43	Chwarta	35.71972	45.57472	1011.6	694.8
14	Gwer	36.04486	43.4808	309.7	235.3	44	Dukan	35.95417	44.95278	700.4	576.4
15	Barzewa	36.6268	44.6333	798.3	721.1	45	Qaladiza	36.1755	45.1333	628.2	681.9
16	Bastora	36.33888	44.16049	630.0	412.4	46	Rania	36.2391	44.8855	607.8	713.9
17	Makhmoor	35.7833	43.5833	287.7	228.2	47	S-sadiq	35.34369	45.85344	544.1	550.2
18	Koya	36.09944	44.64806	724.5	472.2	48	Qaradagh	35.30933	45.38961	887.9	721.7
19	Taqtaq	35.88737	44.58561	397.5	371.1	49	Arbat	35.42462	45.58683	701.6	492.5
20	Shamamk	36.0400	43.84669	310.6	276.2	50	Kani	35.38498	45.70458	685.8	498.7
21	(DU)	36.8679	42.97900	588.3	495.1	51	Byara	35.22507	46.11625	1333.5	656.3
22	Semel	36.87333	42.85400	491.6	414.4	52	Mawat	35.90074	45.4105	1063.8	712.0
23	Zakho	37.14361	42.68191	501.4	528.7	53	Darband	35.11626	45.68625	534.6	557.9
24	Batel	36.95946	42.72165	531.0	435.5	54	Chamcha	35.53333	44.83333	726.6	427.0
25	Dam-DU	36.87576	43.0029	605.6	514.2	55	Kalar	34.6411	45.32927	243.2	304.7
26	Dar. Hajam	37.19878	42.82273	649.8	509.5	56	Agjalar	35.74827	44.89741	702.3	390.0
27	zaxo-farh	37.15991	42.65873	447.1	525.2	57	Bngrd	36.06601	45.02989	841.2	666.7
28	Batifa	37.18404	37.18404	930.2	670.3	58	Sangaw	35.28623	45.1825	704.4	470.8
29	kanimasi	37.22906	37.22906	1332.3	736.2	59	Bawanor	34.82332	45.5087	358.4	364.3
30	Zaweta	36.90583	36.90583	1006.4	723.4	60	Kifri	34.68333	44.96639	238.7	279.2

The study area included Duhok (DU), Erbil (ER), and Sulaimaniyah (SU) governorates of the KRI. It is characterized by significant seasonal variations in precipitation, temperature, potential evaporation, wet winters, and dry summers (Figure 2). Most of the 586 mm precipitation amounts fall from October to May. During the study period between 1998 and 2017, the highest average monthly rainfall was 134.3 mm, in January. The highest average monthly evaporation rate was in July, with 250 mm in ER. The highest average monthly temperature recorded in July was 41.21 °C in Erbil, while the lowest monthly temperature was in January that reached 2.13 °C in SU.
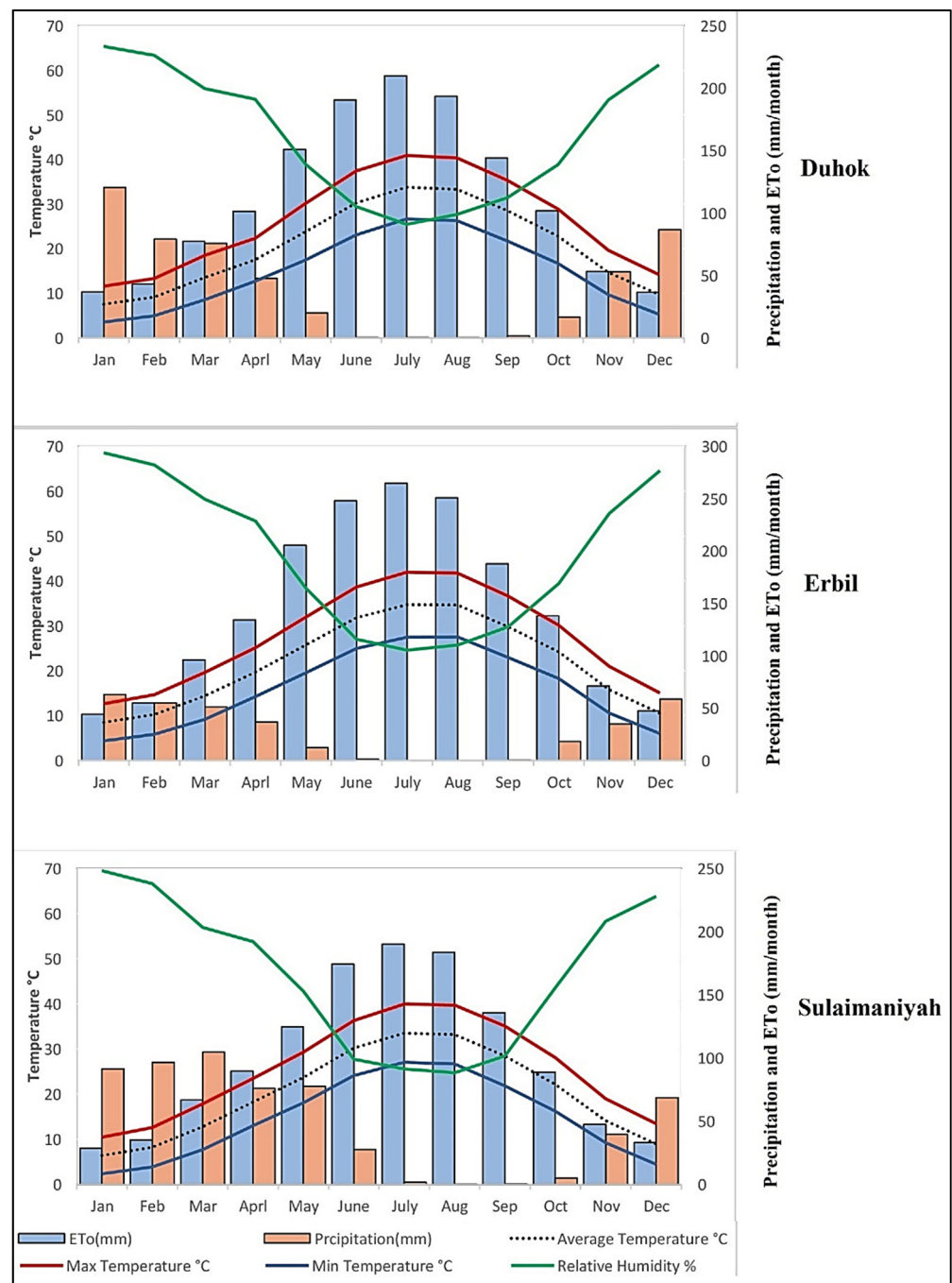
Figure 2. Monthly precipitation, relative humidity, potential evaporation, maximum, minimum, and mean temperature at Duhok (DU), Erbil (ER), Sulaimaniyah (SU), and surrounding areas recorded between 1998 and 2017.

2.2. Data

2.2.1. Landsat Datasets

For this study, 120 Landsat images were downloaded from the U.S. Geological Survey website (https://glovis.usgs.gov/, accessed on 5 January 2022). The images were acquired in April and May of 1997 to 2017, as the highest level of vegetation growth occurs every year in the two months in the study area. The remotely sensed datasets were a collection of three different sensors: L5 Thematic Mapper (TM), L7 Enhanced Thematic Mapper Plus (ETM+), and L8 Operational Land Imager (OLI) with a spatial resolution of 30 m. They were provided in geo-referenced format, cloudless, and free images type with (Path/row

170/34, 170/35, 169/35, 169/34, 168/35, 168/36). The characteristics of the images used in this study are provided in Supplementary Materials Table S1.

2.2.2. Landsat Images Preprocessing

The downloaded images were corrected by calibrating Digital Number (DN) into radiance by using the information from their metadata files. Then, the resultant images were converted into surface reflectance using Envi ver. 5.3. The images were then geo-referenced to the Universal Transverse Mercator (UTM), Zone 38 North with a World Geodetic System (WGS) 84 datum. To get good alignment of pixels in the respective images, an image-to-image registration was performed with a Root Mean Square Error (RMSE) of 0.4 pixels [38].

Six scenes of Landsat images were combined to create a mosaic covering the entire study area for each of the twenty years. The produced mosaic represents and covers the entire land in the KRI and the surrounding areas. The infrared thermal band (6th) of TM/ETM+ and Band 10 of OLI images were utilized for retrieving the LST images, while near-infrared (NIR) and red bands were also applied to calculate the NDVI images [39].

2.2.3. Image Processing
NDVI

The near-infrared (NIR) and red bands were also applied to calculate the NDVI images [39]. The NDVI index is calculated with the aid of the red (Red) and the near-infrared (NIR) bands of the Landsat images, using Formula (1), as follows:

$$NDVI = (NIR - Red)/(NIR + Red) \tag{1}$$

Theoretically, the NDVI values ranged between -1.0 and $+1.0$. However, the typical range of NDVI gauged from vegetation and other earth surface materials is between approximately -0.1 (NIR less than Red) for non-vegetated surfaces and as high as 0.9 for dense vegetative cover. The NDVI values increase with increasing green biomass, positive seasonal changes, and favorable factors (e.g., abundant precipitation) [40,41]. The NDVI-based vegetation density can be classified into three classes based on NDVI values, as shown in Table 2 The USGS remote sensing phenology states the following: Areas of barren rock, sand, or snow usually show very low NDVI values (for example, 0.1 or less) [42]. Sparse vegetation, such as shrubs and grasslands, or senescing crops may result in moderate NDVI values (approximately 0.2 to 0.5). High NDVI values (approximately 0.6 to 0.9) correspond to dense vegetation, such as that found in temperate and tropical forests or crops at their peak growth stage [41–43].

Table 2. Class Classification Standards for Description of NDVI Vegetation Cover.

Class	Class Classification Criterion
Bare soil and/or water (no vegetation)	$NDVI \leq 0$
Very Low NDVI	≤ 0.2
Low to Moderately Low NDVI	$0.2 < NDVI \leq 0.6$
Moderately High to High NDVI	$0.6 < NDVI \leq 1$

LST

The LST fraction images were produced using the Landsat thermal bands, the sixth bands of the L5 TM, L7 ETM+, and the 10–11 of L8 TIRS. Brightness temperature can be calculated using Plank's law using Top of the Atmosphere radiances obtained from TIR sensors [44]. Firstly, we calculated the changes in the five classes of droughts for the study area within 20 years (Figure 3). We then compared the changes among the five drought categories and selected the one which shows the most significant change than the other four categories as the dominating one. The fraction of lands dominated by each drought category is then counted for each period to show the temporal evolutions.

Equations used for converting digital numbers into land surface temperature are presented as follows:

Conversion of thermal DN values into satellite brightness temperature

$$TB = K2/\ln((K1/L\lambda) + 1) \tag{2}$$

One shows the largest change compared to the other four categories. The fraction of lands dominated by each drought category is then counted for each period to show the temporal evolution.

K1 = Band-specific thermal conversion constant (in watts/$m^2 \times$ srad $\times$ μm)

K2 = Band-specific thermal conversion constant (in kelvin)

Lλ is the spectral radiance at the sensor's aperture, measured in watts/($m^2 \times$ star $\times$ μm).

Calculation of the Land Surface Temperature in Kelvin

$$T = TB/[1 + (\lambda \times TB/\varrho) \ln\varepsilon] \tag{3}$$

where λ = wavelength of emitted radiance; ϱ = h × c/σ (1.438 × 10^{-2} m·K); h = Planck's constant (6.626 × 10^{-34} J·s); σ = Boltzmann constant (1.38 × 10^{-23} J/K); c = velocity of light (2.998 × 10^{-8} m/s); ε = emissivity, which is given by the following [45]; ε = 1.009 + 0.047 ln(NDVI).

Conversion from Kelvin to Celsius

$$Tc = T - 273 \tag{4}$$

T = land surface temperature in Kelvin

Tc = land surface temperature in Celsius [44].
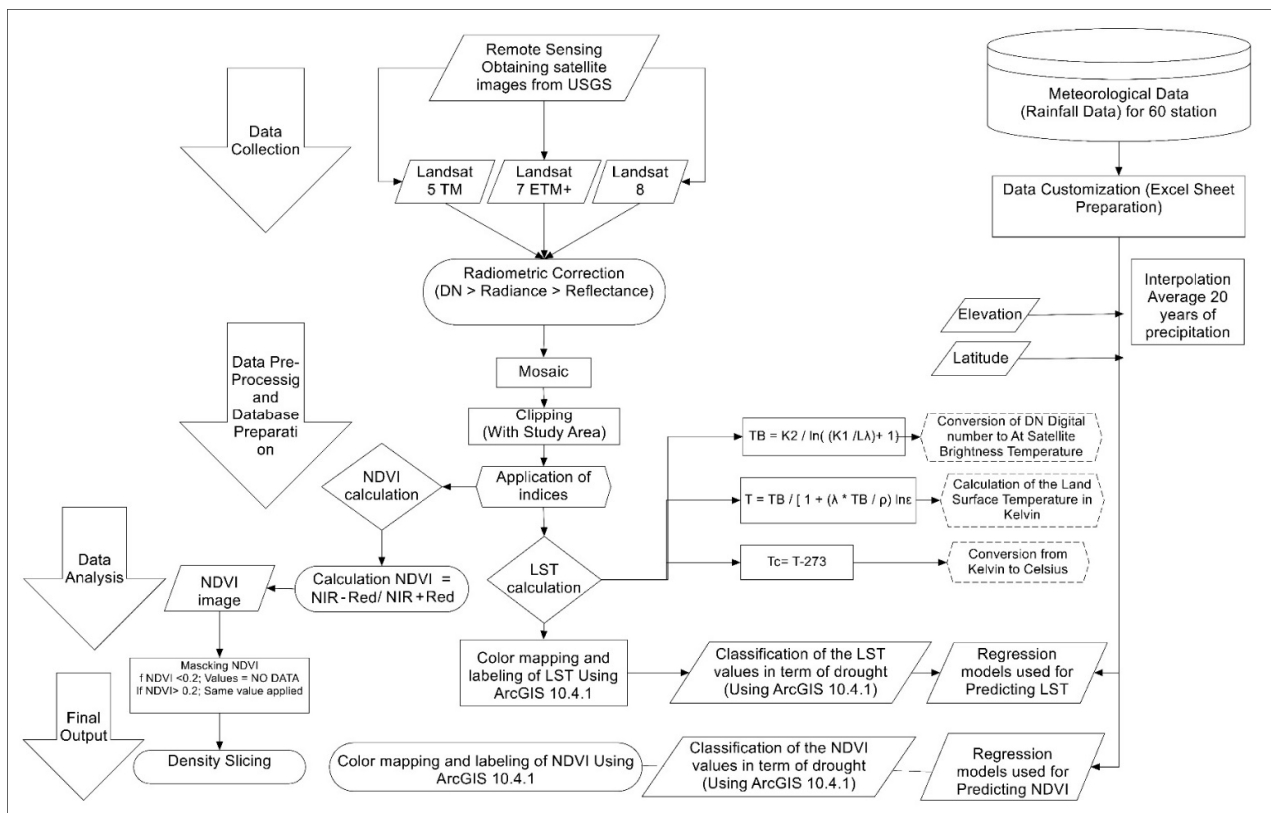
Figure 3. Flowchart of the methodology adopted in this study.

2.3. Statistical Analysis for Time Series

2.3.1. Trend Detection (Mann–Kendall Test)

The nonparametric Mann–Kendall test is commonly employed to detect monotonic trends in time series of environmental data, climate, or hydrological data [46,47]. The Mann–Kendall test is a statistical test widely used for trend analysis in climatological and hydrological time series [48]. There are two advantages of using this test: first, it is a nonparametric test and does not require data to be normally distributed. Second, the test has low sensitivity to abrupt breaks due to inhomogeneous time series [49].

The computational procedure for the Mann–Kendall test considers the time series of n data points and Ti and Tj as two subsets of data where i = 1, 2, 3, . . . , n − 1 and j = i + 1, i + 2, i + 3, . . . , n. The data values are evaluated as an ordered time series. Each data value is compared with all subsequent data values [46,47]. If a data value from a later time period is higher than a data value from an earlier time period, the statistic S is incremented by 1. On the other hand, if the data value from a later time period is lower than a data value sampled earlier, S is decremented by 1. The net result of all such increments and decrements yields the final value of S [50].

The Mann–Kendall's Statistic is computed as follows:

$$S = \sum_{i=1}^{n-1} \sum_{j=i+1}^{n} \text{sign}(Tj - Ti) \tag{5}$$

where Tj and Ti are the annual maximum daily values in years j and i, j > i, respectively.

If n < 10, the value of |S| is compared directly to Mann–Kendall's theoretical distribution of S derived, the two-tailed test is used. At a certain probability level, H0 is rejected in favor of H1 if the absolute value of S equals or exceeds a specified value $S\alpha/2$, where $S\alpha/2$ is the smallest S, which has the probability less than $\alpha/2$ to appear in the case of no trend. A positive (negative) value of S indicates an upward (downward) trend. For n ≥ 10, the statistic S is approximately normally distributed with the mean and variance as follows: E(S) = 0. The variance ($\sigma2$) for the S statistic is defined by the following:

$$\text{sign}(Tj - Ti) = \begin{cases} 1 & \text{if } Tj - Ti > 0 \\ 0 & \text{if } Tj - Ti = 0 \\ -1 & \text{if } Tj - Ti < 0 \end{cases} \tag{6}$$

$$\sigma^2 = \frac{n(n-1)(2n+5) - \sum t_i(i)(ti-1)(2ti+5)}{18} \tag{7}$$

$$Z_s = \begin{cases} \frac{s-1}{\sigma} & \text{for } S > 0 \\ 0 & \text{for } S = 0 \\ \frac{s+1}{\sigma} & \text{for } S < 0 \end{cases} \tag{8}$$

In which ti denotes the number of ties to an extent i. The summation term in the numerator is used only if the data series contains tied values. The standard test statistic Zs is calculated as follows:

Test statistic Z is used as a measure of significance of trend. For example, if −1.96 < Z < 1.96 = No trend, Z > 1.96 = Increase in trend, Z < −1.96 = Decrease in trend [51].

2.3.2. Magnitude of Trend (Sen's Slope)

Sen's slope estimator is a nonparametric, linear slope estimator that works most efficiently on monotonic data. Different linear regression is not significantly affected by gross data errors, outliers, or missing data [47]. Sen's slope method is used to regulate the scale of the trend line. According to Sen's method, this test computes both the slope, i.e., the linear rate of change, and the intercept [51]. First, a set of linear slopes is calculated as follows:

$$dk = Xi - Xi/j - i \tag{9}$$

For $(1 \leq i < j \leq n)$, where d is the slope, X denotes the variable, n is the number of data, and I and j are indices. Sen's slope is then calculated as the median from all slopes:

$$yat = Xt - b \times t \tag{10}$$

b = Median dk. The intercepts are computed for each time step t as given by the following, and the corresponding intercept is as well as the median of all intercepts. This function also computes the Sen's slope's upper and lower confidence limits [47].

2.3.3. Pearson Correlation between Indices and Ecological Parameters

Correlation coefficients were applied for each of NDVI, LST and rainfall, elevation, and latitude for 1998 through 2017. Using bivariate correlation analysis, the strength of the statistical relationships among drought and the individual study variables were computed using SPSS. The correlation matrix allowed us to find the important statistical relationships between NDVI, LST, and the study variables, such as rainfall, elevation, and latitude. A linear relationship between observed and simulated variables was tested by the Pearson correlation coefficient. It has a value range from -1 to $+1$ of which the signs indicate the direction of the relationship, where the absolute value indicates the strength, whereas larger absolute values indicate stronger positive or negative associations [52].

2.3.4. Root Mean Square Error (RMSE) and Coefficient of Residual Mass (CRM)

The (RMSE), also called Root Mean Square Deviation (RMSD), is commonly used to quantify the differences between simulated and actual values, which are called residuals. The RMSE estimates the data scattering to be around a 1:1 relationship, which indicates how much the model under or overestimates the measurements. On the other side, the (CRM) value indicates the model's tendency to over or underestimate the measurements, whereas positive values indicate that the model underestimates the measurements, while negative values indicate an overestimation tendency. For an ideal prediction, RMSE and CRM values should equal 0.0 [53–59].

The RMSE of a model prediction with respect to the estimated variable X model is defined as the square root of the mean squared error:

$$RMAS = \sqrt{\frac{\sum_{i=1}^{n} (X_{obs,i} - X_{model,i})^2}{n}} \tag{11}$$

where Xobs is the observed value, and Xmodel is the modeled value at time/place i.

$$CMR = \frac{\sum_{i=1}^{N} Pi - \sum_{i=1}^{N} Oi}{\sum_{i=1}^{N} Oi} \tag{12}$$

where Pi is the predicted, Oi is the observed, and (i = 1 to N).

3. Results

To better understand NDVI and LST patterns and their relationships, in this study, the produced thematic images were imported into ArcGIS 10.4.1. The resultant maps presented in the following pages show the spatial pattern of vegetation cover according to NDVI, LST, and the spatial distribution of annual precipitation averages from 1998 to 2017, as shown in Table 1.

3.1. NDVI

The NDVI has been widely used to examine the relationship between spectral vegetation variability and vegetation growth rate changes. This study's results revealed that NDVI values varied from the lowest value of 0.13 in 2008 to the highest value of 0.48 in 2014 (Table 3).

Table 3 shows the variation in vegetation status in the KRI from 1998 to 2017. As noted, significant decreases were observed in the area of vegetation in the KRI from 2000 to 2008 due to the extreme and severe years of drought that hit Iraq, which led to decreased agricultural land area. The total vegetation area based on NDVI in 2000 and 2008 was 7225.1 (14.4%) and 20,609.9 km^2 (41.0%), respectively. The vegetation cover has been shrunk by 39% and 13%, respectively, based on the average vegetation area (54%) over 20 years. This decline can be mainly attributed to the severe drought episodes that hit Iraq, including the KRI in 2000 and 2008, among other factors, in addition to a significant drop in rainfall averages. On the other side, the highest NDVI-based vegetation area was recorded in 2016, 32,315.2 km^2 (64.2%), representing an increase of 10% based on the vegetation cover average. From the viewpoint of NDVI values, the lowest values were recorded in 2000, 2008, and 2012 at 0.196, 0.131, and 0.202, respectively. Table 3 shows the area of the NDVI-based vegetation density classes in KRI from 1998 to 2017. In class 1, the results revealed that the largest class area was recorded in 2000 and 2008 by 6050.0 (83.7%) and 16,453.7 km^2 (79.8%), respectively; in addition, the lowest area from class 2 at values 0.2–0.6 were recorded in 2000 and 2008 at 1175.1 (16.3%) and 4156.1 km^2 (20.2%), respectively.

The NDVI results are presented in Table 3 and Figure 4, which show the spatial variation of the NDVI-based vegetation classes in the study area from 1998 to 2017. The maps show the impact of drought on the vegetation density in the KRI, whereas it severely impacted some parts of the southern KRI, while there was no impact (no drought) or a slight drought in the northeast parts of the study area. The NDVI results showed that the drought intensity in the KRI gradually increases toward the southwest parts. The drought regions belonging to class 1 (values < 0.2) are a large and continuous distribution. Table 3 and Figure 4 display the actual drought status episodes in 2000, 2008, and 2012 in the KRI. Precisely, the NDVI-based low-vegetation class increased in the three drought years to be 6050.0 (83.7%), 16,453.7 (79.8%), and 14,024.1 km^2 (53.1%) in 2000, 2008, and 2012, respectively. The maps in Figure 4 disclose that the years 2000 and 2008 were the drier years in the KRI, particularly in the southern parts.

Table 3. The max, min, mean, and std. dev. of NDVI values and the area of vegetative cover and the NDVI-Based Vegetation Density Classes in KRI from 1997 to 2017.

					Class 1		Class 2		Class 3					
					Values < 0.2		0.2 < Values ≤ 0.6		0.2 < Values < 1					
					Very Low NDVI		Low to Moderately Low NDVI		Moderately High to High NDVI		Total Vegetative Cover			
Years	Max.	Min.	Mean	Std. Dev.	Area (km^2)	Area (%)	Area (km^2)	Area (%)	Area (km^2)	Area (%)	(km^2)	(%)	(±%)	Total Study Area (km^2)
1998	0.99	0.10	0.27	0.13	9890.0	37.5	16,075.4	60.9	417.8	1.6	26,383.2	52.4	−1.6	53,000
1999	0.98	0.10	0.23	0.10	12,881.7	46.1	14,994.2	53.7	70.2	0.3	27,946.0	55.5	1.5	53,000
2000	0.99	0.02	0.20	0.13	6050.0	83.7	1175.1	16.3	0	0.0	7225.1	14.4	−39	53,000
2001	0.73	0.03	0.22	0.13	14,859.6	50.0	14,707.5	49.5	169.3	0.6	29,736.4	59.1	5	53,000
2002	0.73	0.06	0.23	0.12	14,320.6	47.6	15,741.6	52.3	51.3	0.2	30,113.5	59.8	5.8	53,000
2003	0.72	0.05	0.24	0.12	12,635.4	43.6	16,319.1	56.3	49.4	0.2	29,003.9	57.6	3.6	53,000
2004	0.72	0.04	0.21	0.12	15,076.6	49.9	15,109.7	50.0	11.3	0.0	30,197.6	60	6	53,000
2005	0.73	0.06	0.20	0.10	14,704.7	55.7	11,702.8	44.3	10.9	0.0	26,418.4	52.5	−1.5	53,000
2006	0.78	0.02	0.21	0.14	14,744.0	51.7	13,699.3	48.1	67.8	0.2	28,511.1	56.7	2.6	53,000
2007	0.73	0.11	0.29	0.11	7802.9	25.7	22,419.1	73.9	110.2	0.4	30,332.3	60.3	6.2	53,000
2008	0.64	0.02	0.13	0.09	16,453.7	79.8	4156.1	20.2	0.1	0.0	20,609.9	41	−13	53,000
2009	0.85	0.08	0.26	0.11	9091.2	36.3	15,910.7	63.6	35.4	0.1	25,037.3	49.7	−4.3	53,000
2010	0.72	0.13	0.28	0.11	7873.5	27.3	20,994.2	72.7	27	0.1	28,894.7	57.4	3.4	53,000
2011	0.76	0.06	0.22	0.13	15,185.5	56.4	11,670.7	43.4	61.3	0.2	26,917.5	53.5	−0.6	53,000
2012	0.72	0.01	0.20	0.13	14,024.1	53.1	12,340.4	46.7	36.9	0.1	26,401.4	52.5	−1.6	53,000
2013	0.63	0.16	0.29	0.09	4636.1	16.5	23,491.1	83.5	0.3	0.0	28,127.6	55.9	1.8	53,000
2014	1.00	0.29	0.48	0.12	5674.20	18.4	25,152.7	81.6	0.0	0.0	30,826.8	61.3	7.2	53,000
2015	0.64	0.18	0.31	0.08	2076.6	6.5	29,782.4	93.5	2.2	0.0	31,861.2	63.3	9.3	53,000
2016	0.72	0.18	0.30	0.08	2984.6	9.2	29,325.5	90.8	5.1	0.0	32,315.2	64.2	10.2	53,000
2017	0.64	0.18	0.28	0.07	21.4	0.1	26,111.7	96.4	963.6	3.6	27,096.8	53.8	−0.2	53,000
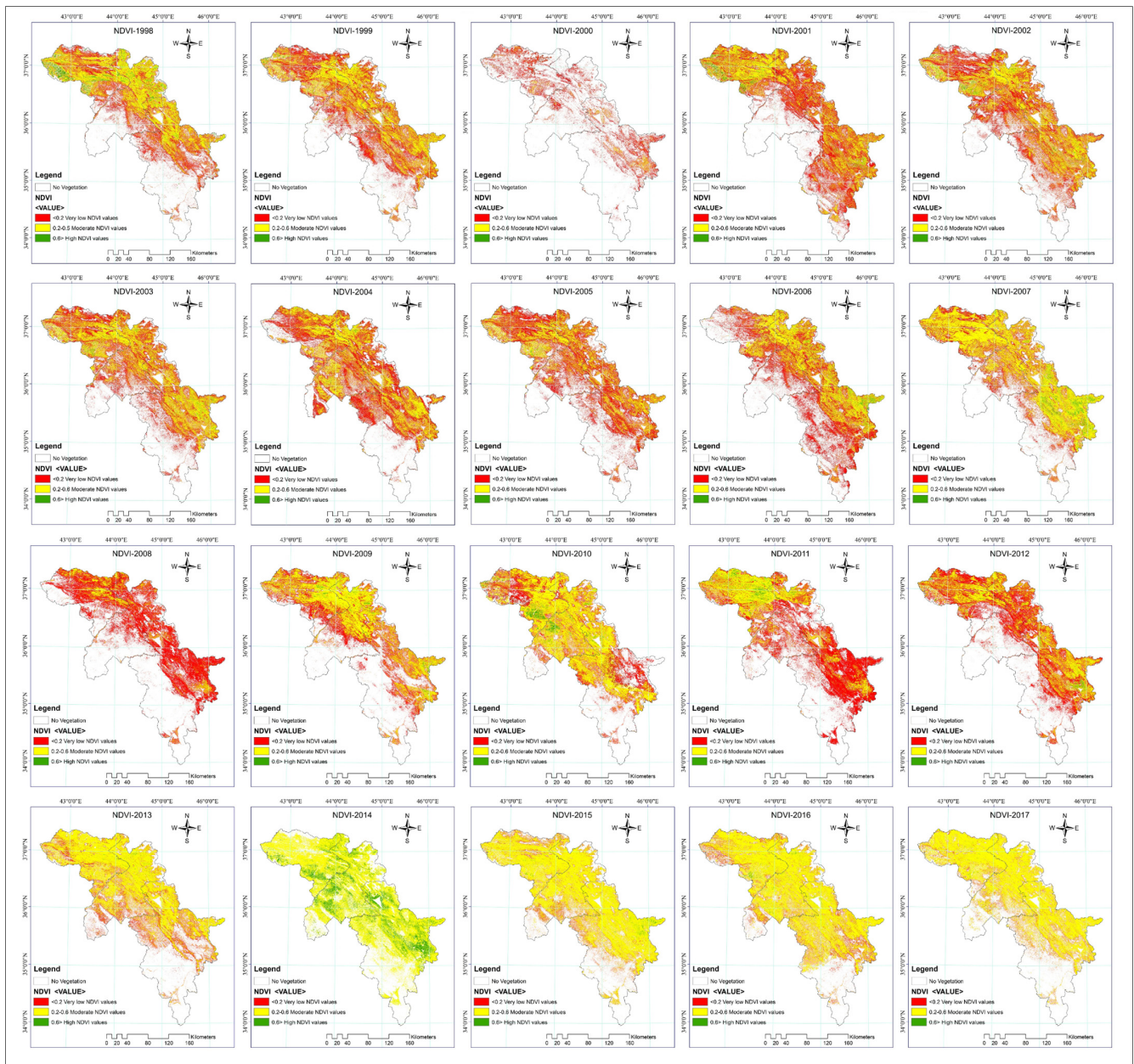
Figure 4. Spatial Variation of the NDVI-Based Vegetation in 1998 to 2017.

The NDVI values were the lowest in the southwest and west parts of the region compared to the northeastern parts, with higher vegetation and a higher NDVI value (Figure 4). There was a significant decline in annual rainfall averages in some sites in KRI compared to rainfall averages of the other studied locations from 1998 to 2017. Figures 5 and 6 shows the minimum values of NDVI-based vegetation cover due to the changes in precipitation rates, whereas precipitation averages were low in some locations (Table 1). On the other side, the precipitation averages were high in some sites, which positively reflected the increase in NDVI values (Figure 4). Low precipitation and high temperature play a negative role in decreasing NDVI values and vegetation cover in the southwest parts of KRI during growing seasons.
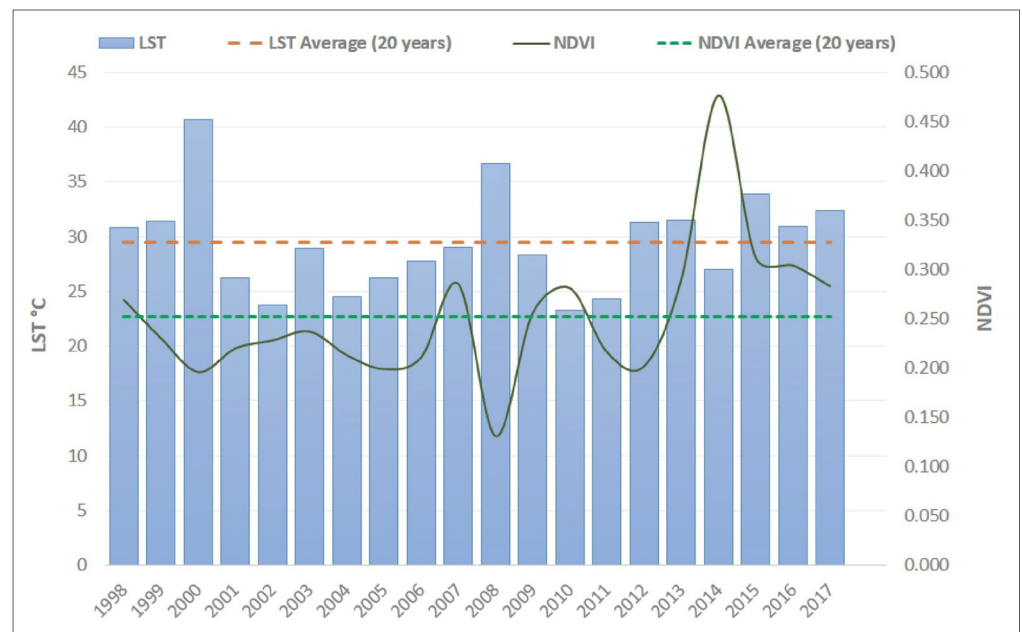
Figure 5. Average values of LST and NDVI in the study area (1998–2017).
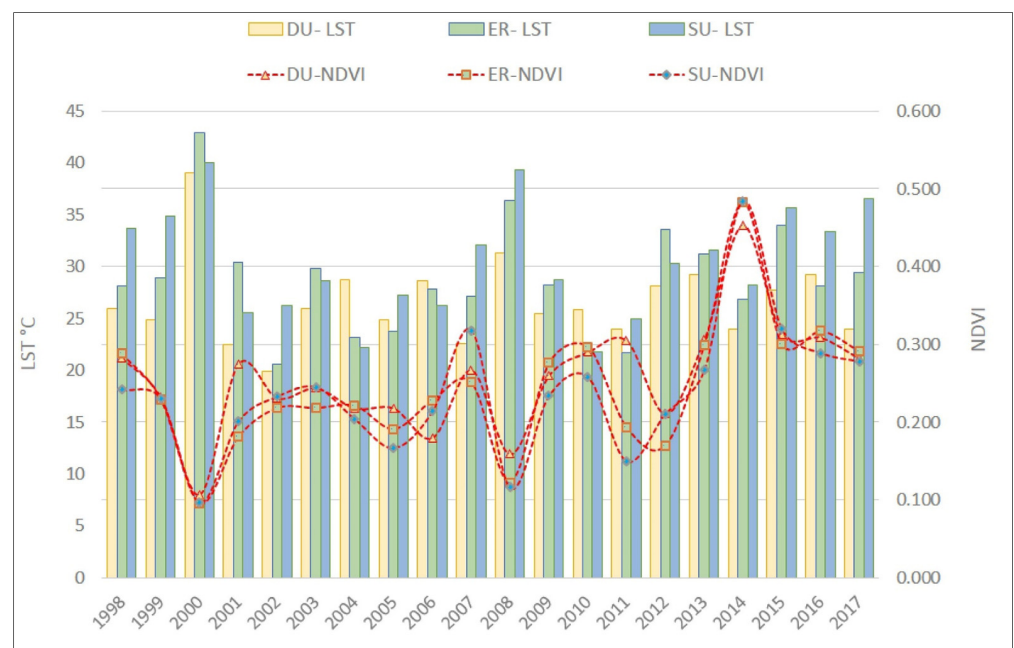
Figure 6. Average values of LST and NDVI in the ER, SU, and DU governorates (1998–2017).

3.2. LST

The LST fraction images were derived using thermal infrared (TIR) of Landsat imagery, which can be utilized to express the land surface temperature and indicate drought status [60]. The LST status of the study area in the period 1998–2017 is given in Figures 5 and 6 and Table 4. Firstly, we calculated the changes in the five classes of droughts for the study area in 20 years (Figure 3). In this study, the changes in the five drought categories were compared. The category in which the greatest change occurred was compared to the other four categories, and it was considered a comparative treatment. Then, we calculated each drought category area to show the temporal changes. Figure 5 shows the LST mean values of each year of the study period compared with the LST average of the 20 years in the KRI from 1998 to 2017. The temperature rate of KRI showed a steady increase, but the

degree of temperature in the years 2002 (23 °C) and 2010 (22 °C) experienced a downward trend. On the other hand, the LST degree of 2000 and 2008 in KRI was about 41 and 37 °C, respectively. The LST rate increased sharply throughout the period, exceeding those of the years 2002 and 2010.

Table 4 indicates that in 2000 and 2008, the highest LST value area was in class 5, which was more than 40 °C. The study results revealed that a very severe drought hit 27,660.7 km^2 (55.0%) of the total area in class 5 ≥ 40 °C. While in the year 2008, they faced severe heat in 19,261.1 km^2 (38.23%) of class 5 ≥ 40 °C. However, the lowest temperatures were recorded in 2002, 2003, 2004, 2010, 2011, and 2014, which was no higher than 0.4% of the total study area.

Table 4. LST Categories Derived from Landsat Thermal Bands for the Years 1998–2000 and Drought Severity Areas (in km^2) and Percentage based on the LST Index.

Year	Class 1 <10 °C		Class 2 10–20 °C		Class 3 20–30 °C		Class 4 30–40 °C		Class 5 > 40 °C	
	Area (km^2)	Area (%)	Area (km^2)	Area (%)	Area (km^2)	Area (%)	Area (km^2)	Area (%)	Area (km^2)	Area (%)
1998	864.3	1.7	2914.5	5.8	19,465.7	38.7	23,901.7	47.5	3181.5	6.3
1999	972.8	1.9	4379.3	8.7	15,646.5	31.1	23,061.8	45.8	6267.1	12.5
2000	424.9	0.8	321.0	0.6	3135.3	6.2	18,785.7	37.3	27,660.7	55.0
2001	589.6	1.2	8546.9	17.0	26,527.3	52.7	14,639.5	29.1	24.2	0.0
2002	1892.9	3.8	14,647.2	29.1	25,793.2	51.3	7,968.2	15.8	26.0	0.1
2003	424.9	0.8	3509.7	7.0	26,701.8	53.1	19,629.0	39.0	62.2	0.1
2004	2106.9	4.2	10,379.9	20.6	31,040.3	61.7	6,588.5	13.1	211.9	0.4
2005	1208.7	2.4	6545.3	13.0	32,586.4	64.7	9,785.2	19.4	202.0	0.4
2006	291.9	0.6	3702.6	7.4	32,097.4	63.8	14,184.1	28.2	51.6	0.1
2007	388.6	0.8	4378.6	8.7	28,483.9	56.6	13,110.3	26.0	3966.2	7.9
2008	881.4	1.8	1547.2	3.1	8150.3	16.2	20,487.5	40.7	19,261.1	38.3
2009	530.7	1.1	6669.1	13.3	25,221.3	50.1	15,938.3	31.7	1968.1	3.9
2010	1471.7	2.9	14,943.1	29.7	29,135.4	57.9	4,642.8	9.2	134.6	0.3
2011	1021.7	2.0	11,501.9	22.9	31,743.5	63.1	6,038.5	12.0	22.0	0.0
2012	223.7	0.4	1737.1	3.5	19,951.8	39.6	22,213.8	44.1	6201.3	12.3
2013	219.6	0.4	1692.6	3.4	17,799.6	35.4	30,154.3	59.9	461.5	0.9
2014	1148.9	2.3	4866.5	9.7	27,964.0	55.6	16,251.3	32.3	96.8	0.2
2015	478.2	1.0	1213.3	2.4	14,941.8	29.7	25,203.0	50.1	8491.2	16.9
2016	810.0	1.6	1483.8	2.9	22,040.9	43.8	21,873.4	43.5	4119.5	8.2
2017	1895.0	3.8	3650.5	7.3	15,964.2	31.7	20,770.0	41.3	8048.0	16.0

Over 20 years, vast areas in the southern part of Erbil and Sulaimaniyah governorates were affected by very severe drought episodes, while most of the other parts of the study area were characterized by slight and moderate droughts based on LST (Figure 7). The southern parts of the study area were warmer compared to the other parts. The mean values of LST in 2000 and 2008 were 40.7 and 36.0 °C, respectively. This significant increase in surface temperature is due to the lack of rainfall, which led to a lack of moisture and lower vegetation cover area that was mostly found in lands with lower elevation. One of the results of the increase in LST surface temperature in the southeast and southwest of the study area is the decrease in vegetation cover represented by NDVI in the study area. This indicates the negative impact of the high LST on the vegetation growth environment that led to the shrinkage in the vegetation area (NDVI) of the region. In the northeast of the study area, only a few sites had increases in precipitation rates and decreases in the LST values, which in turn was reflected in a vegetation increase (NDVI) at those sites (Figures 5 and 6).
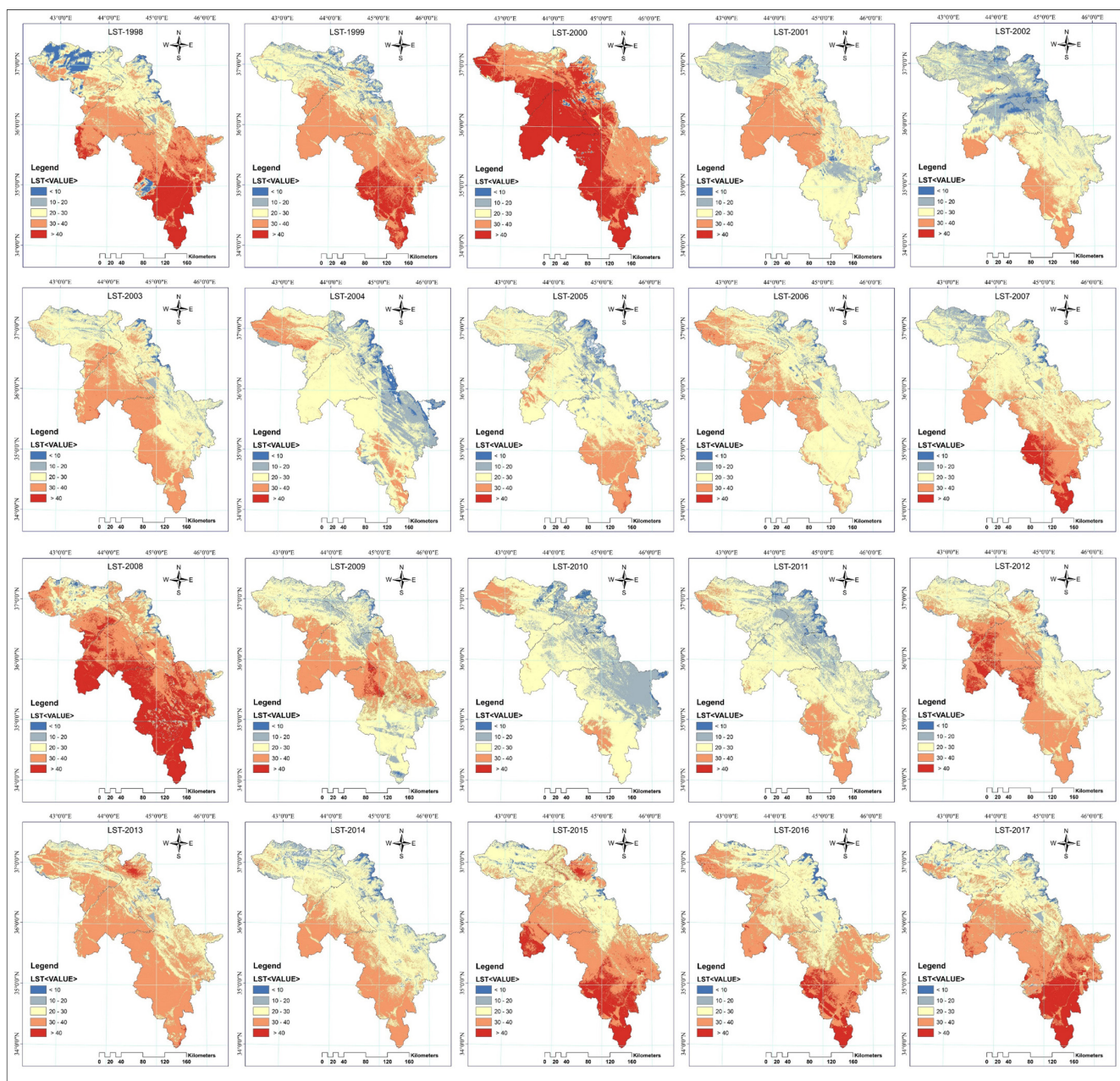
Figure 7. Drought Severity Categories based on LST Index in Years 1998–2017.

3.3. Pearson Correlation Matrix between Indices and Ecological Parameters

Correlation coefficients between latitude, elevation, rainfall, NDVI, and LST during the years from 1998 to 2017 (average of 20 years) are calculated using SPSS and are presented in Table 5. The analysis of variance for the drought indices showed significant differences at $p < 0.01$ and $p < 0.05$ among the analyzed years. The relationship between precipitation, elevation, NDVI, and LST was tested from 1998 to 2017 through Pearson correlation analysis, and the results are presented in Table 5 and Figures 8 and 9. The results showed a significant negative correlation between NDVI and precipitation with LST. On the other hand, there was a positive correlation between NDVI and precipitation (Table 5 and Figures 8 and 9). The correlation between spectral indices based on remote sensing and precipitation was statistically significant. LST and NDVI space's concept refers to the relationship between NDVI with LST, and vegetation abundance was first formulated by Lambing and Ehrlich (1996) with LST plotted as a function of NDVI [61]. In Figures 5 and 6, the lowest values

of NDVI were observed in 2000 and 2008 with higher LST during 2000 and 2008 in ER, DU, and SU (Figure 5). The relationship between the mean and area of NDVI and LST is repeatedly negative.
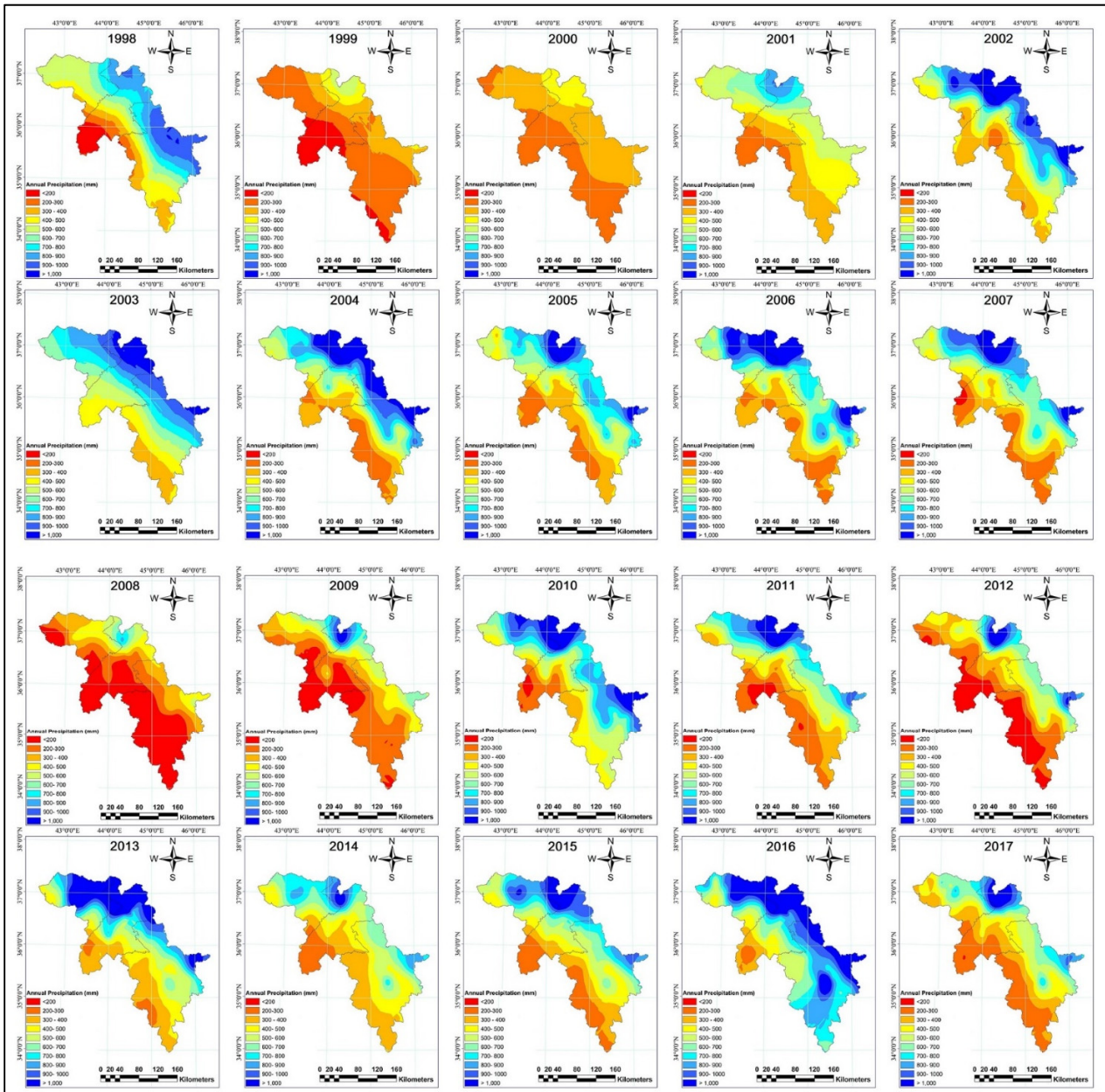
Figure 8. The spatiotemporal distribution of annual precipitation (mm/year) in IKR during the period 2008–2017.

Table 5. Pearson correlation between NDVI, LST, and ecological parameters.

	Longitude	Latitude	Elevation	Rainfall	LST	NDVI
Longitude	1					
Latitude	−0.81 **	1				
Elevation	0.2	0.25	1			
Rainfall	0.14	0.34 **	0.80 **	1		
LST	0.14	−0.59 **	−0.78 **	−0.83 **	1	
NDVI	−0.03	0.53 **	0.76 **	0.83 **	−0.89 **	1

** Correlation is significant at the 0.01 level (2-tailed). * Correlation is significant at the 0.05 level (2-tailed).
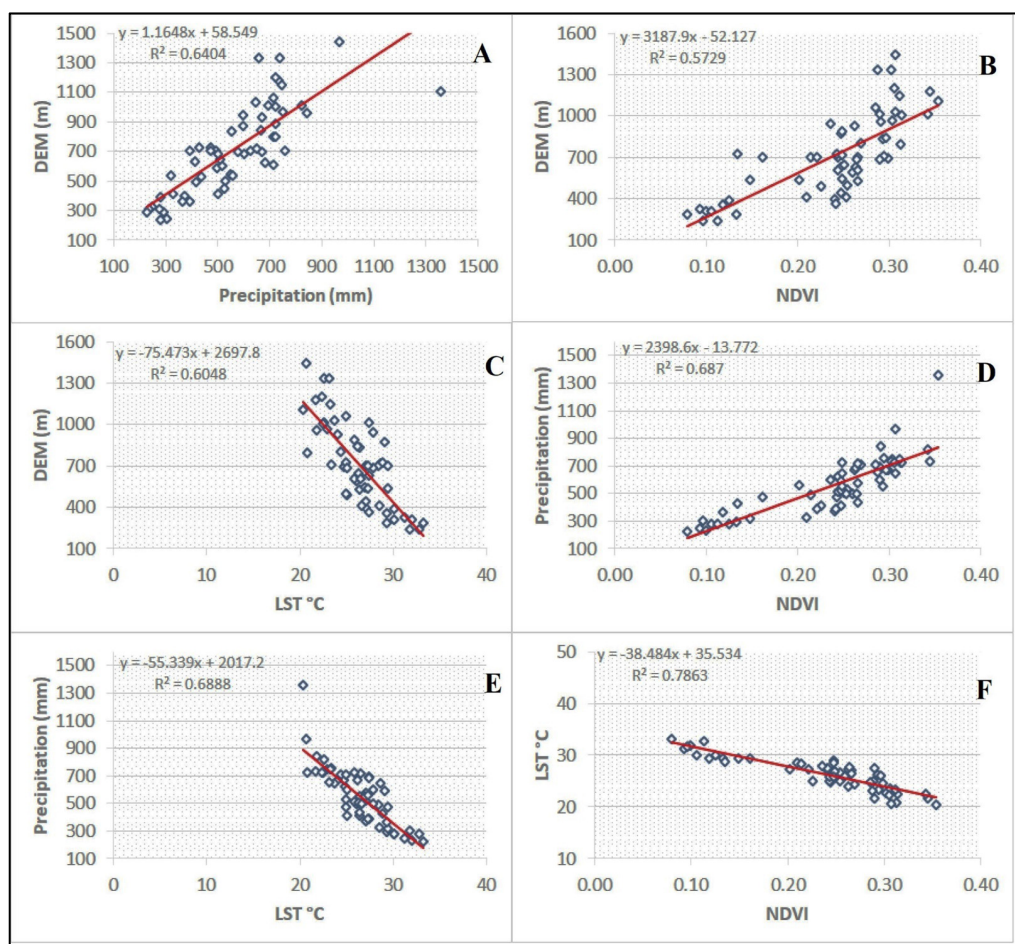
Figure 9. Spatial pattern changes of ecological parameters and drought indices for an average of 20 years in 60 locations. (**A**) Relationships between elevation precipitation. (**B**) Relationships between elevation and NDVI. (**C**) Relationships between elevation and LST. (**D**) Relationships between precipitation and NDVI. (**E**) Relationships between precipitation and LST. (**F**) Relationships between LST and NDVI.

Analysis of variance for the drought indices showed significant differences at $p < 0.01$ and $p < 0.05$ among the analyzed years. The relationship between precipitation, elevation, NDVI, and LST was tested from 1998 to 2017 through Pearson correlation analysis, and the results are presented in Table 5 and Figure 9. The results showed a significant negative correlation between NDVI and precipitation with LST. On the other hand, there was a positive correlation between NDVI and precipitation (Table 5 and Figure 9). The correlation between spectral indices based on remote sensing and precipitation was statistically significant. LST and NDVI space's concept refers to the relationship between NDVI with LST and vegetation abundance was first formulated by Lambing and Ehrlich (1996) with LST plotted as a function of NDVI [61]. In Figures 5 and 6, the lowest values of NDVI were observed in 2000 and 2008 with higher LST during 2000 and 2008 in ER, DU, and SU (Figure 5). The relationship between the mean and area of NDVI and LST is repeatedly negative.

The spatial distributions of the changes in (elevation, precipitation, LST, and NDVI) from 1997 to 2017 are presented in Figure 9A–F. The negative relationships between (NDVI-LST) and (LST-DEM) based on the monthly data from 1998–2017 at 60 different sites were presented in Figure 9C,F. The statistical correlation between (LST-NDVI) was employed to demonstrate the locational variations of temperature effect on vegetation activity. The study's findings also revealed a positive correlation between the LST and NDVI in the northern part of the study area, while the relationship was negative between the mentioned indices at the southern parts.

In general, the three main factors affecting vegetation growth in the study area are the LST, precipitation, and DEM (Figure 8B,D,F). That illustrates the significant shrinking in precipitation averages, the vegetation cover in the southwest, and the considerable increase of vegetation coverage in some of the KRI's northeast parts (Figure 9A,B). Figure 6 shows the significant decreases in LST observed in the country's northeast, caused by increasing NDVI and the precipitation rate. A significant increase was found in the LST values in almost all sites southwest of the KRI, where the vegetation and precipitations are limited. NDVI was sensitive to rainfall and temperature (Figure 9D,E). However, fluctuations were observed in NDVI and LST during the 20 years. The decreases in NDVI were observed during the period LST was increasing in all locations (Figure 9F).

3.4. Trend Analysis of NDVI and LST by Mann–Kendall and Sen's Slope

This study carried out the trend analysis for NDVI and LST in the 60 meteorological stations' locations from 1998 to 2017. MKT and Sen's Slope estimator were used to determine statistical inclining or declining trends. A positive sign indicates an upward slope, while a negative sign represents a downward one. The Sen's slope test results seem to be fairly similar to those obtained from the MKT [52,62].

3.4.1. NDVI

Table 6 indicates the NDVI trends in the KRI through 20 years using the Mann–Kendall test and Sen's slope methods. Out of 60 locations, only 11 recorded significant trends increasing at the 5% level of Sen's estimator of slope following the Mann–Kendall test, which was employed to figure out the change per unit time of trends observed in all NDVI time series. Trends of NDVI have been calculated for each site individually using Sen's magnitude of slope (Q). In the Mann–Kendall test, the Z statistics revealed that the series covers the KRI study area.

The majority of NDVI-based vegetation increases occurred in the northern and northeastern parts. Table 6 reveals the trend analysis results that statistically significant (95% confidence level) positive trends were 2.34, 2.08, 2.21, 2.24, 2.66, 2.24, 3.47, 2.08, 2.17, 2.11, 2.11, 2.5, and 2.17 for Northeast sites, including Khabat, Mergasurer, Barzewa Battle, Zawiya, Mangesh, Kanimasi, Amadea, Bamarni, Bazian, Halabja, Byara, and Mawat.

Table 6. NDVI Trends in the KRI over the 20 Years using the Mann–Kendall Test and Sen's Slope Methods.

Mann–Kendall Trends							Sen's Slope
Time Series Location Name	First Year	Last Year	N	Test Z	Sen's Slope (Q)	Prop.	Trend (at 95% Level of Significance)
Erbil	1998	2017	20	0.68	0.002	0.7522	no trend
Qushtapa	1998	2017	20	1.52	0.005	0.9364	no trend
Khabat	1998	2017	20	2.34	0.008	0.9903	increasing
Bnaslawa	1998	2017	20	1.91	0.006	0.9722	no trend
harir	1998	2017	20	1.65	0.006	0.9510	no trend
Soran	1998	2017	20	1.52	0.006	0.9364	no trend
Shaqlawa	1998	2017	20	1.72	0.005	0.9572	no trend
Khalifan	1998	2017	20	1.65	0.006	0.9510	no trend
choman	1998	2017	20	1.36	0.003	0.9135	no trend
Sidakan	1998	2017	20	1.40	0.004	0.9185	no trend
Rwanduz	1998	2017	20	1.56	0.005	0.9403	no trend
Mergasur	1998	2017	20	2.08	0.007	0.9811	increasing

Table 6. *Cont.*

Time Series Location Name	First Year	Last Year	N	Test Z	Sen's Slope (Q)	Prop.	Trend (at 95% Level of Significance)
				Mann–Kendall Trends			**Sen's Slope**
Dibaga	1998	2017	20	1.20	0.004	0.8850	no trend
Gwer	1998	2017	20	1.04	0.003	0.8504	no trend
barzewa	1998	2017	20	2.21	0.006	0.9863	increasing
Bastora	1998	2017	20	0.97	0.002	0.8348	no trend
Makhmoor	1998	2017	20	1.23	0.004	0.8912	no trend
Koya	1998	2017	20	1.49	0.004	0.9322	no trend
Taqtaq	1998	2017	20	1.91	0.006	0.9722	no trend
Shamamk	1998	2017	20	0.78	0.003	0.7819	no trend
Duhok	1998	2017	20	1.91	0.004	0.9722	no trend
semel	1998	2017	20	1.30	0.005	0.9028	no trend
Zakho	1998	2017	20	1.20	0.003	0.8850	no trend
Batel	1998	2017	20	2.24	0.004	0.9874	increasing
Duhok	1998	2017	20	1.56	0.005	0.9403	no trend
Darkar	1998	2017	20	1.69	0.005	0.9542	no trend
zaxo-farh	1998	2017	20	0.42	0.002	0.6634	no trend
Batifa	1998	2017	20	1.82	0.006	0.9654	no trend
kani masi	1998	2017	20	3.47	0.012	0.9997	no trend
Zaweta	1998	2017	20	2.66	0.007	0.9961	increasing
Mangish	1998	2017	20	2.24	0.008	0.9874	increasing
Deraluke	1998	2017	20	1.98	0.008	0.9761	no trend
Akre	1998	2017	20	1.46	0.004	0.9279	no trend
Amadia	1998	2017	20	2.08	0.005	0.9811	increasing
Sarsink	1998	2017	20	1.20	0.003	0.8850	no trend
Bamarni	1998	2017	20	2.17	0.008	0.9851	increasing
Bardarash	1998	2017	20	0.94	0.003	0.8266	no trend
Qasrok	1998	2017	20	1.78	0.005	0.9628	no trend
SUL	1998	2017	20	1.98	0.005	0.9761	no trend
Bazian	1998	2017	20	2.11	0.005	0.9825	increasing
Halabja	1998	2017	20	2.11	0.005	0.9825	increasing
Penjwen	1998	2017	20	1.91	0.008	0.9722	no trend
Chwarta	1998	2017	20	1.40	0.006	0.9185	no trend
Dukan	1998	2017	20	1.40	0.004	0.9185	no trend
Qaladiza	1998	2017	20	1.27	0.003	0.8971	no trend
Rania	1998	2017	20	1.36	0.003	0.9135	no trend
Said sadiq	1998	2017	20	1.59	0.005	0.9441	no trend
Qaradagh	1998	2017	20	1.33	0.003	0.9083	no trend
Arbat	1998	2017	20	0.91	0.003	0.8182	no trend
mwan	1998	2017	20	1.65	0.004	0.9510	no trend
Byara	1998	2017	20	2.50	0.008	0.9938	increasing
Mawat	1998	2017	20	2.17	0.004	0.9851	increasing
Darbandik	1998	2017	20	1.91	0.005	0.9722	no trend
Chamcha	1998	2017	20	1.20	0.004	0.8850	no trend
Kalar	1998	2017	20	0.97	0.001	0.8348	no trend
Agjalar	1998	2017	20	0.55	0.002	0.7094	no trend
bngrd	1998	2017	20	1.62	0.004	0.9476	no trend
Sangaw	1998	2017	20	1.46	0.005	0.9279	no trend
Bawanor	1998	2017	20	1.49	0.003	0.9322	no trend
Kifri	1998	2017	20	0.71	0.002	0.7623	no trend

Note: $-1.96 < Z < 1.96$ = No trend, $Z > 1.96$ = Increase in trend, $Z < -1.96$ = Decrease in trend.

3.4.2. LST

Table 7 illustrates that a significant trend in LST was 2.04, 2.08, 2.17, 2.01, 1.98, 2.37, 1.98, 2.01, 2.01, and 2.5, for Southwest sites, for Erbil, Qushtapa, Dibaga Gwer, Shamamk, Makhmoor, Mangish, Chamchamal, Kalar, Bawanor and Kifri, respectively. On the other hand, the lower trends were in Northeast sites, including Mangish—2.8, Bamarni—2.11, Penjwen—2.95, Chwarta—2.21, and Byara—2.3.

Table 7. LST trends in the KRI over the 20 years using the Mann–Kendall Test and Sen's slope methods.

	Mann–Kendall Trends						Sen's Slope
Time Series Location Name	First Year	Last Year	N	Test Z	Sen's Slope (Q)	Prop.	Trend (At 95% Level of Significance)
Erbil	1998	2017	20	2.04	0.456	0.9795	increasing
Qushtapa	1998	2017	20	2.08	0.492	0.9811	increasing
Khabat	1998	2017	20	1.10	0.203	0.8650	no trend
Bnaslawa	1998	2017	20	0.71	0.114	0.7623	no trend
harir	1998	2017	20	0.68	0.125	0.7522	no trend
Soran	1998	2017	20	1.07	0.150	0.8578	no trend
Shaqlawa	1998	2017	20	0.58	0.066	0.7204	no trend
Khalifan	1998	2017	20	−0.06	0.000	0.4741	no trend
choman	1998	2017	20	−1.75	−0.242	0.0399	no trend
Sidakan	1998	2017	20	−0.39	−0.051	0.3485	no trend
Rwanduz	1998	2017	20	−0.58	−0.100	0.2796	no trend
Mergasur	1998	2017	20	−1.82	−0.698	0.0346	no trend
Dibaga	1998	2017	20	2.17	0.450	0.9851	increasing
Gwer	1998	2017	20	2.01	0.172	0.9779	increasing
barzewa	1998	2017	20	−1.01	−0.114	0.1573	no trend
Bastora	1998	2017	20	1.85	0.366	0.9678	no trend
Makhmoor	1998	2017	20	2.37	0.264	0.9911	no trend
Koya	1998	2017	20	−1.40	−0.260	0.0815	no trend
Taqtaq	1998	2017	20	0.06	0.010	0.5259	no trend
Shamamk	1998	2017	20	1.98	0.179	0.9761	increasing
Duhok	1998	2017	20	−0.13	−0.025	0.4484	no trend
semel	1998	2017	20	0.13	0.009	0.5516	no trend
Zakho	1998	2017	20	0.10	0.020	0.5388	no trend
Batel	1998	2017	20	−0.03	−0.001	0.4871	no trend
Duhok Dam	1998	2017	20	0.06	0.014	0.5259	no trend
Darkar hajam	1998	2017	20	0.94	0.183	0.8266	no trend
zaxo−farh	1998	2017	20	−1.75	−0.375	0.0399	no trend
Batifa	1998	2017	20	−0.52	−0.087	0.3018	no trend
kani masi	1998	2017	20	−1.52	−0.563	0.0636	no trend
Zaweta	1998	2017	20	−1.33	−0.400	0.0917	no trend
Mangish	1998	2017	20	−2.08	−0.470	0.0189	Decreasing
Deraluke	1998	2017	20	−0.42	−0.065	0.3366	no trend
Akre	1998	2017	20	−1.69	−0.375	0.0458	no trend
Amadia	1998	2017	20	−1.07	−0.240	0.1422	no trend
Sarsink	1998	2017	20	−1.10	−0.285	0.1350	no trend
Bamarni	1998	2017	20	−2.11	−0.717	0.0175	Decreasing
Bardarash	1998	2017	20	0.23	0.031	0.5898	no trend
Qasrok	1998	2017	20	0.29	0.056	0.6149	no trend
Sulaymaniyah	1998	2017	20	0.29	0.045	0.6149	no trend
Bazian	1998	2017	20	−0.78	−0.192	0.2181	no trend
Halabja	1998	2017	20	0.84	0.183	0.8005	no trend
Penjwen	1998	2017	20	−2.95	−0.662	0.0016	Decreasing
Chwarta	1998	2017	20	−2.21	−0.540	0.0137	Decreasing
Dukan	1998	2017	20	0.52	0.065	0.6982	no trend
Qaladiza	1998	2017	20	−1.52	−0.342	0.0636	no trend
Rania	1998	2017	20	−0.32	−0.087	0.3728	no trend
Said sadiq	1998	2017	20	0.42	0.120	0.6634	no trend
Qaradagh	1998	2017	20	−0.23	−0.023	0.4102	no trend
Arbat	1998	2017	20	0.42	0.111	0.6634	no trend
mwan	1998	2017	20	−0.13	−0.034	0.4484	no trend
Byara	1998	2017	20	−2.30	−0.502	0.0106	Decreasing
Mawat	1998	2017	20	−1.85	−0.468	0.0322	no trend
Darbandikhan	1998	2017	20	0.06	0.010	0.5259	no trend
Chamchamal	1998	2017	20	1.98	0.562	0.9761	Increasing
Kalar	1998	2017	20	2.01	0.366	0.9779	Increasing
Agjalar	1998	2017	20	1.43	0.324	0.9233	no trend
bngrd	1998	2017	20	1.27	0.211	0.8971	no trend
Sangaw	1998	2017	20	0.84	0.239	0.8005	no trend
Bawanor	1998	2017	20	2.01	0.454	0.9779	Increasing
Kifri	1998	2017	20	2.50	0.237	0.9938	Increasing

Note: −1.96 < Z < 1.96 = No trend, Z > 1.96 = Increase in trend, Z < −1.96 = Decrease in trend.

3.5. Multiple Regression Statistics, RMSE, and CRM

The Root Mean Square Error (RMSE) value indicates how predicted and observed measurements match, while the Coefficient of Residual Mass (CRM) value measures a model's tendency to over or underestimate the measurements. Positive values for CRM indicate that the model underestimates the measurements, and negative values overestimate [63]. For an ideal fit between the observed and predicted data, RMSE and CRM's values should equal 0.0 [62]. As can be seen from the statistical analysis results, the accuracy of the model in the estimation of NDVI and LST in Tables 8 and 9 for the study periods was tested by calculating the Coefficient of Residual Mass (CRM), Root Mean Square Error (RMSE), and coefficient of determination (R^2), respectively.

The results in Table 8 showed that the NDVI-based vegetation cover was more affected by climatic and topographic factors (precipitation and elevation) in the study area. A high value for multiple regression coefficients indicates strong relationships between the variables, and the low RMSE and CRM values show a reasonable precision and low error of the model. The multiple regression (R), RMSE, and CRM were calculated and presented in Tables 8 and 9. The efficiency and accuracy of the models for predicting drought indices were evaluated using statistical coefficients.

The values of regression parameters were used to predict the drought index (NDVI) in Table 8 from 1998 to 2017. The (R) values ranged from 0.77 in 1998 to 0.87 in 2017, RMSE from 0.039 in 2000 to 0.068 in 2005, and CRM from -0.006 in 2014 to 0.284 in 1998. These results indicate that although the relationship between variables was stronger in 2017, the prediction error was lower in 2008 and 2013. Comparing the observed and simulated measurements, the model gives appropriate predictions of the drought status. Moreover, different time scales were considered in the model. The drought predictions can be more reliable and efficient and ensure that the developed model is suitable and efficient.

The regression analyses in Table 8 showed that the spectral indices were related to total precipitation, geographic elevation, and latitude. The LST values of 1998 to 2017 were (R) ranged from 0.47 in 2001 to 0.85 in 2013, and RMSE were from 2.7 in 1999 to 7.0 in 2000.

Table 8. Parameters of the regression models used for predicting drought index (NDVI) in the KRI.

| | | | $y = \beta_0 + \beta_1 x_1 + \beta_2 x_2 + \beta_3 x_3$ | | | | |
| | | β_0 | β_1 | β_2 | β_3 | | |
Year	**R**	**Intercept**	**x1 Coefficients**	**x2 Coefficients**	**x3 Coefficients**	**RMSE**	**CRM**
1998	0.77	-2.19	6.4×10^{-2}	-9.9×10^{-7}	1.6931×10^{-4}	0.090	0.284
1999	0.80	-1.02	3.0×10^{-2}	9.790×10^{-5}	3.0739×10^{-4}	0.047	0.002
2000	0.80	-1.27	3.5×10^{-2}	5.872×10^{-5}	2.4785×10^{-4}	0.039	0.031
2001	0.72	-0.06	3×10^{-3}	1.0642×10^{-4}	2.1147×10^{-4}	0.062	0.002
2002	0.77	-0.79	2.6×10^{-2}	3.402×10^{-5}	2.0132×10^{-4}	0.056	0.009
2003	0.75	-0.89	2.8×10^{-2}	8.010×10^{-5}	8.339×10^{-5}	0.046	0.000
2004	0.77	-0.94	2.8×10^{-2}	2.258×10^{-5}	2.0384×10^{-4}	0.054	-0.004
2005	0.74	-1.03	2.9×10^{-2}	7.895×10^{-5}	1.7897×10^{-4}	0.068	0.088
2006	0.81	-1.35	4.0×10^{-2}	1.4746×10^{-4}	5.234×10^{-5}	0.050	-0.005
2007	0.76	0.26	-5×10^{-3}	1.1165×10^{-4}	1.6574×10^{-4}	0.056	0.011
2008	0.78	-1.40	3.9×10^{-2}	8.544×10^{-5}	1.2644×10^{-4}	0.043	0.016
2009	0.77	-1.67	4.9×10^{-2}	7.641×10^{-5}	1.7644×10^{-4}	0.057	0.000
2010	0.76	-1.93	5.8×10^{-2}	5.352×10^{-5}	7.833×10^{-5}	0.051	0.006
2011	0.84	-2.12	6.1×10^{-2}	4.172×10^{-5}	1.9596×10^{-4}	0.054	-0.004
2012	0.74	-0.97	2.9×10^{-2}	9.920×10^{-5}	9.931×10^{-5}	0.050	0.004
2013	0.81	-1.84	5.6×10^{-2}	9.731×10^{-5}	4.716×10^{-5}	0.049	0.003
2014	0.73	0.86	-1.9×10^{-2}	1.0719×10^{-4}	2.6338×10^{-4}	0.065	-0.006
2015	0.78	-0.15	8×10^{-3}	9.893×10^{-5}	1.3360×10^{-4}	0.049	0.005
2016	0.84	-0.79	2.7×10^{-2}	1.6592×10^{-4}	4.533×10^{-5}	0.043	0.007
2017	0.87	-0.85	2.6×10^{-2}	1.6069×10^{-4}	1.3260×10^{-4}	0.044	-0.001

Note: When y = NDVI Drought index, x1 = Latitude, x2 = Elevation, x3 = Precipitation.

Figure 10 illustrates the quantile–quantile plots (Q–Q) used to visually examine the degrees of distribution. From the visual point of view, there was little difference when choosing among the various distributions for representing the data used in the study [64]. For instance, the Q–Q plot of observed spectral indices at 60 locations in KRI versus expected values pointed out that NDVI and LST have been fitted to better distributions, as most of the observations fall on and around the straight line and few points are a little bit far away from the fitted line.

Table 9. Parameters of the regression models used for predicting drought index (LST) in KRI.

			$y = β0 + β1\,x1 + β2\,x2 + β3\,x3$		
			β0	β1	β2	β3		
Years	R	Intercept	x1 Coefficients	x2 Coefficients	x3 Coefficients	RMSE	CRM
1998	0.50	200.326	-4.5090×10^{0}	3.79×10^{-3}	-7.70×10^{-3}	3.366	-0.0019
1999	0.74	162.592	-3.6067×10^{0}	-2.98×10^{-3}	-4.37×10^{-3}	2.736	0.0000
2000	0.63	115.233	-1.8216×10^{0}	-1.62×10^{-3}	-2.774×10^{-2}	7.026	-0.0271
2001	0.47	-92.048	3.2245×10^{0}	3.73×10^{-3}	-2.01×10^{-3}	4.823	-0.0374
2002	0.75	161.735	-3.8018×10^{0}	-3.39×10^{-3}	5.0×10^{-4}	2.709	0.0158
2003	0.59	-8.567	1.0771×10^{0}	-1.60×10^{-3}	-4.29×10^{-3}	3.745	-0.1117
2004	0.68	42.094	-3.318×10^{-1}	-4.21×10^{-3}	-8.13×10^{-3}	3.456	-2.95×10^{-5}
2005	0.67	-51.024	5.825×10^{-1}	1.403×10^{-2}	6.25×10^{-3}	5.988	0.0121
2006	0.58	73.968	-1.1655×10^{0}	-5.41×10^{-3}	-2.93×10^{-3}	3.709	-0.0001
2007	0.66	137.659	-2.9794×10^{0}	1.17×10^{-3}	-7.40×10^{-3}	3.568	0.0001
2008	0.52	-71.482	3.0436×10^{0}	1.90×10^{-3}	-2.42×10^{-3}	3.626	-1.17×10^{-5}
2009	0.55	168.828	-3.8644×10^{0}	4.77×10^{-3}	-9.94×10^{-3}	4.759	0.0003
2010	0.75	61.496	-7.443×10^{-1}	-1.6×10^{-4}	-1.737×10^{-2}	4.132	-0.0002
2011	0.65	110.496	-2.2353×10^{0}	-5.50×10^{-3}	-1.06×10^{-3}	3.189	-0.0001
2012	0.75	88.654	-1.4965×10^{0}	-6.09×10^{-3}	-5.20×10^{-3}	2.774	0.0031
2013	0.85	36.517	1.13×10^{-2}	1.11×10^{-3}	-1.716×10^{-2}	3.840	-0.0109
2014	0.83	130.942	-2.6048×10^{0}	-6.98×10^{-3}	-1.367×10^{-2}	3.522	0.0026
2015	0.80	169.176	-3.6726×10^{0}	-1.752×10^{-2}	3.63×10^{-3}	4.159	-6.24×10^{-5}
2016	0.82	109.215	-1.9879×10^{0}	-5.89×10^{-3}	-1.167×10^{-2}	3.797	-0.0090
2017	0.79	200.224	4.4465×10^{0}	-1.164×10^{-2}	-4.23×10^{-3}	4.413	0.0008

Note: When y = LST Drought Index, x1 = Latitude, x2 = Elevation, x3 = Precipitation.
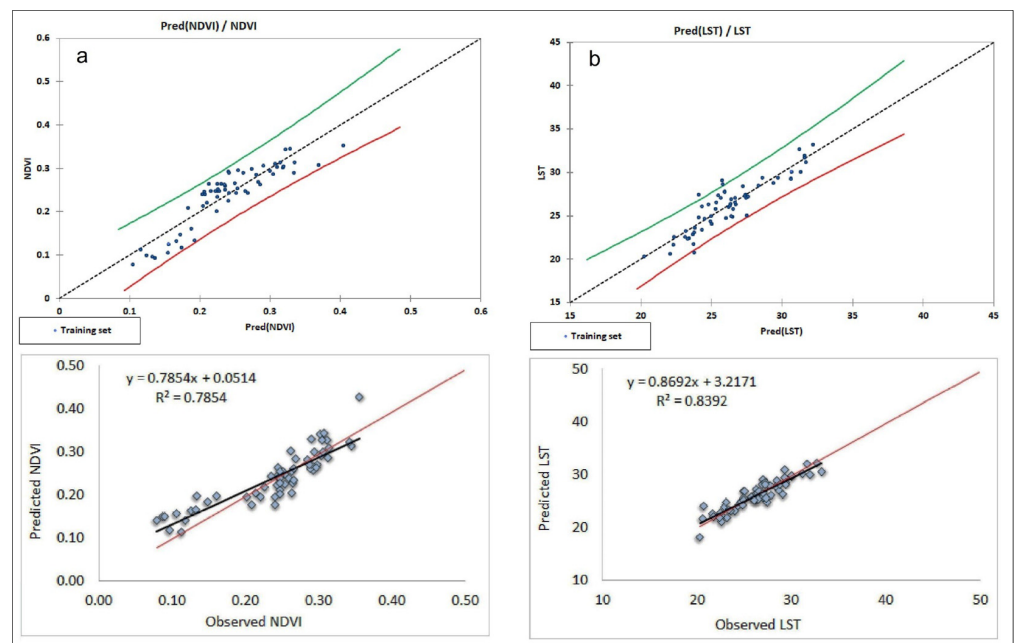
Figure 10. The Quantile–Quantile Plot (Q–Q Plot) of Observed (**a**) NDVI and (**b**) LST at 60 Locations Versus Predicted Values.

4. Discussion

NDVI and LST maps of the consecutive 20 years clearly show the onset and extent of drought. According to the results shown in Table 3 and Figure 4, it can be said that the studied region has faced drought episodes over the study period, especially in the years 2000 and 2008. The Mann–Kendall test assessed changes in drought indices at the 60 sites. The multiple regression for the 20 years was used to understand variable climatic influences on droughts and temporal variations and their relationships with precipitation changes, altitude, and latitude. A considerable change in NDVI values and LST was strongly observed in 2000 and 2008. These results correspond to the study conducted by [65,66], whereas the year 2008 was the driest year during the study period. The occurrence of drought is associated with reduced vegetation area and NDVI mean values. However, LST values increased throughout the 20 years of study, particularly in 2000 and 2008 [12].

The NDVI value indicates very low vegetation, especially in the southern part of the study area (Figure 4 and Table 3). These results correspond to the study conducted by [34], whereas both of them found that year 2008 had the most severe drought year during the study period. Ref. [67] assessed the spatiotemporal changes in drought in Iraq using SPI from 1980 to 2010. They found that drought caused deterioration from normal to extreme levels in Iraq during 2000, 2008, and 2010 (which was the driest year), while NDVI coverage was high in the northern part of the study area in the identified period [66]. The northern part of the study area is characterized by a topography covered with grasses and trees, while the density of NDVI-based vegetation is less in the middle part and lesser in the southern part [25]. The less extensive coverages of precipitation are observed in the southern part of the study area in the KRI (Figures 2C and 8).

The terrain, trees, and shrub area may play an essential role in assessing the vegetation increase due to the progress of laws on the protection of the environment and the prevention of logging in the last ten years, as well as the improvement of the living costs and raising awareness of the people living in these areas and continuous artificial afforestation in that area [68]. After investigating drought vicissitudes in KRI changes with NDVI and LST variation, we observed droughts' vicissitudes in terms of frequency, duration, and intensity. Specifically, we first calculated the changes in classes (classes 1, 2, and 3) for NDVI and classes 1, 2, 3, 4, and 5 for LST. Then, we compared the changes among the five drought categories and selected the one that shows the largest change compared to the other four categories as the dominant one. The percentage of lands dominated by each drought category was counted for each period to show the temporal evolution.

Based on the drought index scale, areas affected by drought have low NDVI [41]. NDVI values indicated that the southwestern and western parts of KRI experienced drought (Figures 4 and 5). However, its magnitude and spatial extension varied. Low values indicated the dry season, while high values indicated the wet season [69]. The values varied spatially and temporally across the region from 1998 to 2017 (Figures 3 and 4). This was mainly because of the precipitation amount, frequency, and intensity [70]. The variation in NDVI is controlled by meteorological variables, such as precipitation, temperature, and relative humidity [41]. The NDVI values were spatially varied due to climate, soil, and topographic variability.

The southern region shows a net decrease of its vegetative cover during the considered time range. It seems to be affected by land-degradation processes caused by droughts, which are an issue in this area [13]. It cannot be expected to perceive differences in the vegetation or physiological (decrease or increase of certain strata) density with slight accuracy. However, it seems to have been shown that the main decreased features of vegetation are in the southern part of KRI. All correlations between the monthly index values and meteorological parameters from the different locations are statistically significant at 95%. The spatial patterns of droughts for the growing seasons in April showed rainfall decreases, and LST values increase in the growing seasons led to an NDVI value reduction in the southwest parts of the KRI. Thus, the increase in rainfall and the slight increase in LST caused NDVI to rise at a few locations in the northeast. The direction or absence of

vegetation trends often matches the precipitation trend. This indicates that the combined effect of precipitation and temperature played an important role in decreasing NDVI values and the area of vegetation in the southwest of KRI during the growing season [12].

The increases in LST in the south and southeast parts were due to the lack of vegetation cover and the soil's relative humidity due to the rainfall deficiency in these areas. These areas have led to continuous land and crop degradation and yield losses. The increased temperatures can cause severe natural effects on the environment, including hydrological drought (IPCC, 2012) [71]. The increase of LST is assumed to negatively affect vegetation strength and cause plant stress [69]. The mean LST increases in almost all parts of the KRI, and the minimum LST increases in the mountains. In the eastern parts, maximum LST increases in the southwestern parts of KRI. This trend pattern corresponds with the variation in NDVI (see Figures 5–7). While the lack of precipitation is often the primary cause of drought, increased potential evapotranspiration is linked to temperature and relative humidity [72]. Actual evapotranspiration is additionally controlled by soil moisture, which constitutes a limiting factor for further drying under drought conditions and other processes impacting vegetation development and phenology; for instance, the temperature is also relevant [70,73,74]. Another LST study by Robaa and AL-Barazanji [75] showed that after 1995, the rising trend of the annual mean temperature over Iraq was about 0.5 °C/decade.

In Table 5, the correlation matrix investigates the generality of the represented LST and NDVI relationship with respect to drought monitoring and assessment; LST and NDVI relations show negative correlations in the study area. Usually, the relationship between NDVI and LST is negative, as the value of NDVI increases with decreases in LST. The LST–NDVI correlations are generally negative [39,76]. In the northeast and south parts, where precipitation increased at some locations, there were significant changes in NDVI, except for an insignificant increase at some sites. Increases were observed in the NDVI for the study period except in 2000, 2008, and 2012. A sharp increase between 2000 and 2008 was observed for LST.

Precipitation was gradually increased with the increase in NDVI in the northern parts of KRI. This increase has resulted in an increasing trend in the northeast's NDVI values and vegetation area. On the other hand, continuous increases in LST and decreasing precipitation resulted in continuous decreases in NDVI in the region's southern locations. This indicates that LST was crucial to decreasing NDVI in these areas during the growing season. Figures 4–7 show a constant variability in terrestrial ecosystems at different spatial and temporal scales because of natural and/or anthropogenic causes. The droughts in semi-arid areas significantly contribute to environmental degradation, as they limit the development of vegetation cover and expose the soil to erosion [77].

The spatiotemporal variability of the LST–NDVI relationship on continental or global scales has been investigated in several studies [78,79] and was based on the assumption that complementary information in these studies may provide a more robust characterization for different phenomena at the land's surface. Studies have revealed a strong negative correlation between NDVI and LST resulting from canopy transpiration's cooling effects. This study's NDVI varied due to temporal and spatial variability in rainfall [80,81]. Therefore, NDVI is a relatively good indicator of drought in KRI, and warmer temperatures are more favorable for vegetation growth [82]. Therefore, the application of empirical NDVI–LST-based indices must be limited to areas and periods where negative correlations are observed and not on a global scale. The mean NDVI indicating the vegetation's greenness was strongly related to seasonal rainfall, which indicates the possibility of using NDVI to predict drought [83]. In general, prior studies suggest that the LST–NDVI slope sign may be governed by whether vegetation growth is water-limited (negative slope) or energy-temperature limited (positive slope). The latter is prevalent at high latitudes or in the evergreen tropical forests, whereas the latter may occur at lower latitudes, especially in dry lands [84,85]. A statistical trend test provides more reliable ways to describe trends in long time series than linear regression. Moreover, the *p*-values for the Mann–Kendall

test are calculated. The Mann–Kendall statistics are shown in Table 5. Only 11 locations (Khabat, Mergasur, Barzewa, Batel, Mangish, Deraluke, Amadia, Bazian, Halabja, Mawat, and Darbandikhan) out of 60 showed an upward trend in NDVI.

The Mann–Kendall statistics are shown in Table 7. Nine locations show statistically significant upward trends in LST (Erbil, Qushtapa, Dibaga, Gwer, Shamamk, Chamchamal, Kalar, Bawanor, and Kifri). These results are in accordance with the findings of Razvanchy [86]. Generally, the southern parts of the study area are warmer. In particular, the temperature rise in the southern zone of the region is the lowest of precipitation and low-vegetation cover and elevation and correlated to a statistically downward trend in annual precipitation Figure 9 and Table 7. Multiple regression analysis revealed that the correlation between rainfall, elevation, and latitude with spectral indices is significant during the beginning of the growing season, whereas other biophysical variables play a lesser role. One of the study objectives was to examine the feasibility of regression analysis to make NDVI and LST forecasts.

A time series of drought indices provides a framework for evaluating drought parameters of interest. In order to quantify the prediction accuracy and precision of the model, the (R), RMSE, and CRM were calculated (see Tables 7 and 8). Some statistical coefficients evaluated the efficiency and accuracy of models used for predicting drought indices. Weather and climate phenomena reflect the interaction of dynamic and thermodynamic processes over a wide range of spatial and temporal scales. This complexity results in highly variable atmospheric conditions, including temperatures, motions, and precipitation; events include the persistence of drought conditions over decades of timescales. Thus, rainfall is associated with both altitude and position [25]. However, this explanation for the spatial distribution of precipitation was supported by dense vegetation in mountain areas, where oak forests were more intense than the other areas. In contrast, the northeastern region dominated the study area at a certain height. However, it became less after the first or second hill, and in the plains of Erbil and Sulaimaniyah, where winter crops are cultivated, which are sensitive to high temperatures and low precipitation [87,88].

5. Conclusions

This study assessed droughts status changes during 20 years of growing seasons in the KRI. This study contributes to drought severity assessment by quantifying NDVI decrease and LST increase during long-term climate. The resultant maps show the change pattern in the relationship between remote sensing-based drought indices and climate factors. From this study, the following points can be concluded:

Severe drought circumstances prevailed during 2000 and 2008 over a large KRI area. The onset and extent of drought can be clearly observed through NDVI, LST, and precipitation maps for the studied 20 years. The land-cover classification shows that the vegetation coverage area was more seriously affected by climatic factors (precipitation and temperature), especially in 2000 and 2008. Considering the significant recurrence of drought, it is crucial to satisfy the water needs of the study area by using other available water resources, such as groundwater, for supplementary irrigation in the rainfed areas of the southern part of KRI. The correlation between LST and NDVI in the same measured year was significant, likely due to the delayed effect of scarce precipitation on vegetation. More detailed investigations are needed to understand the frequency of drought and its relationship to factors affecting it.

Landsat-based spectral drought indices were significantly correlated with precipitation, geographical elevation, and latitude. High values of multiple correlation and regression indicate strong relationships between the variables, and the low RMSE and CRM values show a reasonable precision and a low error of the resultant model. Comparing the results obtained for the modeling indicates that the presented model gives appropriate predictions of the drought situation. Moreover, different time scales were considered in the model so that the drought predictions can be more reliable and efficient, and the developed model is ensured to be suitable and efficient.

Acute water stress was evident all over the study area in 2000, 2008, and 2012. Despite the prevalence of drought conditions over a large area of KRI during the mentioned years, some areas in the eastern part of the region remained unaffected by the lack of precipitation and water stress. Those areas are characterized by humid and sub-humid climate types, which helps keep the area green even during the drought year.

Spatial variation in the NDVI and LST resulted from the uneven distribution of rainfall and geographical elevation effects in the study area. Since the region receives much higher monsoonal rainfall than the western part, even in the drought year, it remains suitable for tree and shrub growth. Unlike the meteorological data available from sparsely distributed meteorological stations, remote sensing meteorological data and remote sensing-based indices can be successfully used to delineate the spatiotemporal extent of drought. In the future, studies may incorporate agricultural production and surface evaporation data to evaluate further the mechanisms by which these factors interact during periods of drought. Due to the large local spatial variation in rainfall, NDVI values also show a high variation, ranging from a low area of 14.4% (7225.1 km^2) in 2000 to 64.2% (32,315.2 km^2) in 2016 (Table 3). On the other hand, LST indicates an upward slope in 2000, 2008, and 2012. The regression model parameters for predicting drought indices from this dataset were disabled to determine the annual precipitation or elevation playing a significant role in the yearly trends in NDVI and LST.

Supplementary Materials: The following are available online at https://www.mdpi.com/article/10.3390/w14060927/s1, Table S1. Landsat data chosen for analysis were a mixture of Landsat TM5, TM7 and OLI8.

Author Contributions: Conceptualization, A.M.F.A.-Q., H.A.A.G. and K.M.; Data curation, H.A.A.G. and A.M.F.A.-Q.; Formal analysis, H.A.A.G. and A.M.F.A.-Q.; Investigation, A.M.F.A.-Q., C.R. and H.A.A.G.; Methodology, H.A.A.G. and A.M.F.A.-Q.; Resources, A.M.F.A.-Q., C.R., K.M. and H.A.A.G.; Supervision, A.M.F.A.-Q.; Validation, H.A.A.G. and A.M.F.A.-Q.; Visualization, A.M.F.A.-Q., C.R. and H.A.A.G.; Writing—original draft, A.M.F.A.-Q. and H.A.A.G.; Review, editing, improving, A.M.F.A.-Q.,C.R and K.M. All authors have read and agreed to the published version of the manuscript.

Funding: This study has been funded by Nuffic, the Orange Knowledge Programme, through the OKP-IRA-104278 project titled "Efficient water management in Iraq switching to climate smart agriculture: capacity building and knowledge development" coordinated by Wageningen University & Research, The Netherlands and Salahaddin University, Erbil, Kurdistan Region, Iraq.

Institutional Review Board Statement: Not applicable.

Informed Consent Statement: Not applicable.

Data Availability Statement: Some data in this manuscript were obtained from the Ministry of Agriculture and Water Resources, Kurdistan Region, Iraq, and the other data from the United States Geological Service (USGS) for providing the Landsat images freely on their web-site, and Statistical analysis of the parameters.

Acknowledgments: The authors would like to thank the United States Geological Service (USGS) for providing the Landsat images freely on their website. The authors would like to thank Tariq Hamakareem Kakahama and Fuad Mohamed Ahmad from the College of Agricultural Engineering Sciences, Salahaddin University, for their sincere assistance. We are also thankful to Nuffic, the Orange Knowledge Programme, through the OKP-IRA-104278, Wageningen University & Research, The Netherlands, the Ministry of Agriculture and Water Resources, Salahaddin University, and the Tishk International University, Erbil, Kurdistan Region, Iraq, for their valuable support.

Conflicts of Interest: The authors declare no conflict of interest.

References

1. Aadhar, S.; Mishra, V. Data Descriptor: High-resolution near real-time drought monitoring in South Asia. *Sci. Data* **2017**, *4*, 170145. [CrossRef] [PubMed]
2. Dubovyk, O. The role of Remote Sensing in land degradation assessments: Opportunities and challenges. *Eur. J. Remote Sens.* **2017**, *50*, 601–613. [CrossRef]

3. Rajsekhar, D.; Singh, V.P.; Mishra, A.K. Multivariate drought index: An information theory based approach for integrated drought assessment. *J. Hydrol.* **2015**, *526*, 164–182. [CrossRef]

4. Lloyd-Hughes, B. The impracticality of a universal drought definition. *Theor. Appl. Climatol.* **2014**, *117*, 607–611. [CrossRef]

5. Yan, G.; Liu, Y.; Chen, X. Evaluating satellite-based precipitation products in monitoring drought events in southwest China. *Int. J. Remote Sens.* **2018**, *39*, 3186–3214. [CrossRef]

6. Al-Quraishi, A.M.F.; Negm, A.M. *Environmental Remote Sensing and GIS in Iraq*; Springer Water; Springer: Cham, Switzerland, 2019; ISBN 9783030213435.

7. Schucknecht, A.; Erasmi, S.; Niemeyer, I.; Matschullat, J. Assessing vegetation variability and trends in north-eastern Brazil using AVHRR and MODIS NDVI time series. *Eur. J. Remote Sens.* **2013**, *46*, 40–59. [CrossRef]

8. Van Loon, A.F.; Gleeson, T.; Clark, J.; Van Dijk, A.I.J.M.; Stahl, K.; Hannaford, J.; Di Baldassarre, G.; Teuling, A.J.; Tallaksen, L.M.; Uijlenhoet, R.; et al. Drought in the Anthropocene. *Nat. Geosci.* **2016**, *9*, 89. [CrossRef]

9. Keyantash, J.A.; Dracup, J.A. An aggregate drought index: Assessing drought severity based on fluctuations in the hydrologic cycle and surface water storage. *Water Resour. Res.* **2004**, *40*, 1–14. [CrossRef]

10. Wilhite, D.A.; Pulwarty, R.S. *Drought and Water Crises*; Routledge: London, UK, 2017; ISBN 9781138035645.

11. UNESCO (United Nations Educational, Scientific and Cultural Organization). *Integrated Drought Risk Management*; UNESCO: Paris, France, 2014.

12. Fadhil, A.M. Drought mapping using Geoinformation technology for some sites in the Iraqi Kurdistan region. *Int. J. Digit. Earth* **2011**, *4*, 239–257. [CrossRef]

13. Andrieu, J. Phenological analysis of the savanna–forest transition from 1981 to 2006 from Côte d'Ivoire to Benin with NDVI NOAA time series. *Eur. J. Remote Sens.* **2017**, *50*, 588–600. [CrossRef]

14. IdRC. *Capacity Assessment for Drought Risk Management in Iraq*; Final Report; Submitted to: United Nations Development Programme (UNDP); Interdisciplinary Research Consultants (IdRC): Amman, Jordan, 2012.

15. Al-Quraishi, A.M.F.; Gaznayee, H.A.A.; Messina, J. Drought severity trend analysis based on the Landsat time-series dataset of 1998–2017 in the Iraqi Kurdistan Region. *IOP Conf. Ser. Earth Environ. Sci.* **2021**, *779*, 012083. [CrossRef]

16. Wu, W.; Muhaimeed, A.S.; Al-Shafie, W.M.; Al-Quraishi, A.M.F. Using L-band radar data for soil salinity mapping—A case study in Central Iraq. *Environ. Res. Commun.* **2019**. [CrossRef]

17. Haktanir, K. *Environmental Challenges in the Mediterranean 2000–2050*; Springer: Berlin/Heidelberg, Germany, 2004. [CrossRef]

18. Harun, R.; Muresan, I.C.; Arion, F.H.; Dumitras, D.E.; Lile, R. Analysis of factors that influence the willingness to pay for irrigation water in the Kurdistan Regional Government, Iraq. *Sustainablity* **2015**, *7*, 9574–9586. [CrossRef]

19. Fadhil, A.M. Sand dunes monitoring using remote sensing and GIS techniques for some sites in Iraq. In Proceedings of the 3rd International Conference on Photonics and Image in Agriculture Engineering (PIAGENG 2013), Sanya, China, 27–28 January 2013. [CrossRef]

20. Awchi, T.A.; Jasim, A.I. Rainfall Data Analysis and Study of Meteorological Draught in Iraq for the Period 1970–2010. *TKRIit J. Eng. Sci.* **2017**, *24*, 110–121. [CrossRef]

21. Hameed, H. Water Harvesting in Erbil Governorate, Kurdistan Region, Iraq Detection of Suitable Sites Using Geographic Information System and Remote Sensing. Master's Thesis, Lund University, Lund, Sweden, 2013.

22. Mohammed, R.; Scholz, M. Adaptation Strategy to Mitigate the Impact of Climate Change on Water Resources in Arid and Semi-Arid Regions: A Case Study. *Water Resour. Manag.* **2017**, *31*, 3557–3573. [CrossRef]

23. Yao, Y.; Qin, Q.; Fadhil, A.M.; Li, Y.; Zhao, S.; Liu, S.; Sui, X.; Dong, H. Evaluation of EDI derived from the exponential evapotranspiration model for monitoring China's surface drought. *Environ. Earth Sci.* **2011**, *63*, 425–436. [CrossRef]

24. Zewdie, W.; Csaplovics, E. Remote sensing-based multi-temporal land cover classification and change detection in northwestern Ethiopia. *Eur. J. Remote Sens.* **2015**, *48*, 121–139. [CrossRef]

25. Al-Quraishi, A.M.F.; Gaznayee, H.A.A.; Crespi, M. Drought Trend Analysis in Sulaimaniyah (Iraqi Kurdistan Region) for the Period 1998–2017 using Remote Sensing and GIS. *J. Arid. Land* **2020**, *3*, 413–430.

26. Dabrowska-Zielinska, K.; Kogan, F.; Ciolkosz, A.; Gruszczynska, M.; Kowalik, W. Modelling of crop growth conditions and crop yield in Poland using AVHRR-based indices. *Int. J. Remote Sens.* **2002**, *23*, 1109–1123. [CrossRef]

27. Abdel-Hamid, A.; Dubovyk, O.; Graw, V.; Greve, K. Assessing the impact of drought stress on grasslands using multi-temporal SAR data of Sentinel-1: A case study in Eastern Cape, South Africa. *Eur. J. Remote Sens.* **2020**, *53*, 1–14. [CrossRef]

28. Alqasemi, A.S.; Hereher, M.E.; Al-Quraishi, A.M.F.; Saibi, H.; Aldahan, A.; Abuelgasim, A. Retrieval of monthly maximum and minimum air temperature using MODIS aqua land surface temperature data over the United Arab Emirates. *Geocarto Int.* **2021**. *ahead of print*. [CrossRef]

29. Vicente-Serrano, S.M.; Beguería, S.; López-Moreno, J.I. A multiscalar drought index sensitive to global warming: The standardized precipitation evapotranspiration index. *J. Clim.* **2010**, *23*, 1696–1718. [CrossRef]

30. Owrangi, M.A.; Adamowski, J.; Rahnemaei, M.; Mohammadzadeh, A.; Sharifan, R.A. Drought Monitoring Methodology Based on AVHRR Images and SPOT Vegetation Maps. *J. Water Resour. Prot.* **2011**, *3*, 325–334. [CrossRef]

31. Wan, Z.; Wang, P. International Journal of Remote Using MODIS Land Surface Temperature and Normalized Difference Vegetation Index products for monitoring drought in the southern Great Plains, USA. *Int. J. Remote Sens.* **2004**, *25*, 37–41. [CrossRef]

32. Heydari, H.; Zoej, M.J.V.; Maghsoudi, Y.; Dehnavi, S. An investigation of drought prediction using various remote-sensing vegetation indices for different time spans. *Int. J. Remote Sens.* **2018**, *39*, 1871–1889. [CrossRef]

33. Karim, T.H.; Keya, D.R.; Amin, Z.A. Temporal and spatial variations in annual rainfall distribution in erbil province. *Outlook Agric.* **2018**, *47*, 59–67. [CrossRef]

34. Eklund, L.; Persson, A.; Pilesjö, P. Cropland changes in times of conflict, reconstruction, and economic development in Iraqi Kurdistan. *Ambio* **2016**, *45*, 78–88. [CrossRef] [PubMed]

35. Eklund, L.; Abdi, A.; Islar, M. From Producers to Consumers: The Challenges and Opportunities of Agricultural Development in Iraqi Kurdistan. *Land* **2017**, *6*, 44. [CrossRef]

36. Saeed, M.A. Analysis of Climate and Drought Conditions in the Fedral. *J. Int. Sci. Environ.* **2012**, *2*, 953.

37. Ministry of Planning-KRG. *Regional Development Strategy for Kurdistan Region. 2012–2016 Final report 2017*; Ministry of Planning-KRG: Erbil, Iraq, 2017.

38. *Module ENVI Atmospheric Correction Module: QUAC and FLAASH User's Guide*; Module Version; ITT Visual Information Solutions: Boulder, CO, USA, 2009; 44p.

39. Sun, Q.; Tan, J.; Xu, Y. An ERDAS image processing method for retrieving LST and describing urban heat evolution: A case study in the Pearl River Delta Region in South China. *Environ. Earth Sci.* **2009**, *59*, 1047–1055. [CrossRef]

40. Rouse, W.; Haas, H.; Deering, W. Monitoring Vegetation Systems in the Great Plains With Erts. In Proceedings of the 3rd Earth Resource Technology Satellite (ERTS) Symposium, Washington, DC, USA, 10–14 December 1973; Volume 1, pp. 48–62.

41. Aquino, D.d.N.; Neto, O.C.d.R.; Moreira, M.A.; dos S. Teixeira, A.; de Andrade, E.M. Use of remote sensing to identify areas at risk of degradation in the semi-arid region. *Rev. Cienc. Agron.* **2018**, *49*, 420–429. [CrossRef]

42. Nath, B.; Acharjee, S. Forest Cover Change Detection using Normalized Difference Vegetation Index (NDVI): A Study of Reingkhyongkine Lake's, Adjoining Areas. *Indian Cartogr.* **2013**, *XXXIII*, 348–403.

43. Di Gregorio, A. *Land Cover Classification System*; FAO: Rome, Italy, 2005; ISBN 9251053278.

44. Dash, P.; Göttsche, F.M.; Olesen, F.S.; Fischer, H. Land surface temperature and emissivity estimation from passive sensor data: Theory and practice-current trends. *Int. J. Remote Sens.* **2002**, *23*, 2563–2594. [CrossRef]

45. Sun, D.; Kafatos, M. Note on the NDVI-LST relationship and the use of temperature-related drought indices over North America. *Geophys. Res. Lett.* **2007**, *34*, 1–4. [CrossRef]

46. Qutbudin, I.; Shiru, M.S.; Sharafati, A.; Ahmed, K.; Al-Ansari, N.; Yaseen, Z.M.; Shahid, S.; Wang, X. Seasonal Drought Pattern Changes Due to Climate Variability: Case Study in Afghanistan. *Water* **2019**, *11*, 1096. [CrossRef]

47. Pohlert, T. Package 'trend': Non-Parametric Trend Tests and Change-Point Detection. *R Packag.* **2016**, 26. [CrossRef]

48. Lu, Y.; Jiang, S.; Ren, L.; Zhang, L.; Wang, M.; Liu, R.; Wei, L. Spatial and Temporal Variability in Precipitation Concentration over Mainland China, 1961–2017. *Water* **2019**, *11*, 881. [CrossRef]

49. U.S. Army Corps of Engineers. *Mann-Kendall Analysis Mann-Kendall Analysis for the Fort Ord Site*; HydroGeoLogic, Inc.—OU-1 Annual Groundwater Monitoring Report—Former Fort Ord, California; HydroGeoLogic, Inc.: Herndon, VA, USA, 2005.

50. Gilbert, R.O. Statistical Methods for Environmental Pollution Monitoring. *Stat. Methods Environ. Pollut. Monit.* **1987**, 204–224.

51. Partal, T.; Kahya, E. Trend analysis in Turkish precipitation data. *Hydrol. Process.* **2006**, *20*, 2011–2026. [CrossRef]

52. Batool, N.; Shah, S.A.; Dar, S.N.; Skinder, S. Rainfall variability and dynamics of cropping pattern in Kashmir Himalayas: A case study of climate change and agriculture. *SN Appl. Sci.* **2019**, *1*, 606. [CrossRef]

53. Jiao, W.; Tian, C.; Chang, Q.; Novick, K.A.; Wang, L. A new multi-sensor integrated index for drought monitoring. *Agric. For. Meteorol.* **2019**, *268*, 74–85. [CrossRef]

54. Yao, X.; Yao, X.; Jia, W.; Tian, Y.; Ni, J.; Cao, W.; Zhu, Y. Comparison and intercalibration of vegetation indices from different sensors for monitoring above-ground plant nitrogen uptake in winter wheat. *Sensors* **2013**, *13*, 3109–3130. [CrossRef] [PubMed]

55. Dutta, D.; Kundu, A.; Patel, N.R. Predicting agricultural drought in eastern Rajasthan of India using NDVI and standardized precipitation index. *Geocarto Int.* **2013**, *28*, 192–209. [CrossRef]

56. Gessner, U.; Machwitz, M.; Conrad, C.; Dech, S. Estimating the fractional cover of growth forms and bare surface in savannas. A multi-resolution approach based on regression tree ensembles. *Remote Sens. Environ.* **2013**, *129*, 90–102. [CrossRef]

57. Lehnert, L.W.; Meyer, H.; Wang, Y.; Miehe, G.; Thies, B.; Reudenbach, C.; Bendix, J. Retrieval of grassland plant coverage on the Tibetan Plateau based on a multi-scale, multi-sensor and multi-method approach. *Remote Sens. Environ.* **2015**, *164*, 197–207. [CrossRef]

58. Li, X.; Zhang, Y.; Bao, Y.; Luo, J.; Jin, X.; Xu, X.; Song, X.; Yang, G. Exploring the best hyperspectral features for LAI estimation using partial least squares regression. *Remote Sens.* **2014**, *6*, 6221–6241. [CrossRef]

59. Peres, L.F.; DaCamara, C.C. Land surface temperature and emissivity estimation based on the two-temperature method: Sensitivity analysis using simulated MSG/SEVIRI data. *Remote Sens. Environ.* **2004**, *91*, 377–389. [CrossRef]

60. Gutman, G.G. Towards Monitoring Droughts from Space. *J. Clim.* **2002**, *3*, 282–295. [CrossRef]

61. Lambin, E.F.; Ehrlich, D. The surface temperature-vegetation index space for land cover and land-cover change analysis. *Int. J. Remote Sens.* **1996**, *17*, 463–487. [CrossRef]

62. Aliyu, S.; Bello, S. Performance Assessment of Hargreaves Model in Estimating Global Solar Radiation in Sokoto, Nigeria. *Int. J. Adv. Sci. Res. Eng.* **2018**, *3*, 6–15. [CrossRef]

63. Park, H.; Kim, K.; Lee, D.K. Prediction of severe drought area based on random forest: Using satellite image and topography data. *Water* **2019**, *11*, 705. [CrossRef]

64. Population, N. Quantile-Quantile Plot (QQ-plot) and the Normal Probability Plot Section 6-6. *Norm. Probab. Plot.* **2012**, *2377*, 1–8.

65. Almamalachy, Y. Utilization of Remote Sensing in Drought Monitoring Over Iraq. Master's Thesis, Portland State University, Portland, OR, USA, 2017. Paper 3996. [CrossRef]

66. Mustafa, Y.T. Spatiotemporal Analysis of Vegetation Cover in Kurdistan Region-Iraq using MODIS Image Data. *J. Appl. Sci. Technol. Trends* **2020**, *1*, 1–6. [CrossRef]

67. Al-timimi, Y.K.; George, L.E.; Al-jiboori, M.H. Drought Risk Assessment in Iraq using Remote Sensing and GIS Techniques. *Iraqi J. Sci.* **2012**, *53*, 1078–1082.

68. Mustafa, Y.T. *Mapping and Estimating Vegetation Coverage in Iraqi Kurdistan Region using Remote Sensing and GIS*; Iraq-Final Report; Prepared and Implemented by Applied Remote Sensing & Gis (Ars&Gis) Center, University Of Zakho, Salahaddin University, University of Garmian, and Directorate of Forests and Range in Duhok; General Directorate of Horticulture, Forestry and Rangeland, Ministry of Agriculture and Water Resources: Erbil, Kurdistan Region, Iraq, 2015; pp. 1–136.

69. Anyamba, A.; Tucker, C.J. Historical perspectives on AVHRR NDVI and vegetation drought monitoring. *Remote Sens. Drought Innov. Monit. Approaches.* **2012**, 23–49. [CrossRef]

70. Wang, J.; Wang, J.; Rich, P.M.; Price, K.P. Temporal responses of NDVI to precipitation and temperature in the central Great Plains, USA. *Int. J. Remote Sens.* **2003**, *24*, 2345–2364. [CrossRef]

71. AlJawa, S.B.; Al-Ansari, N. Open Access Online Journal of the International Association for Environmental. *Hydrol. Assess. Groundw. Qual. Using* **2017**, *26*, 1–14.

72. Oku, Y.; Ishikawa, H.; Haginoya, S.; Ma, Y. Recent trends in land surface temperature on the Tibetan Plateau. *J. Clim.* **2006**, *19*, 2995–3003. [CrossRef]

73. Koundouri, P.; Karousakis, K.; Assimacopoulos, D.; Jeffrey, P.; Lange, M. Water Management in Arid and Semi-Arid Regions. In *Water Management in Arid and Semi-Arid Regions*; Northampton, Mass Edward Elgar: Cheltenham, UK, 2006; ISBN 9781845429973.

74. Zhang, Y.; Wang, X.; Li, C.; Cai, Y.; Yang, Z.; Yi, Y. NDVI dynamics under changing meteorological factors in a shallow lake in future metropolitan, semi-arid area in North China. *Sci. Rep.* **2018**, *8*, 1–13. [CrossRef]

75. Robaa, S.M.; Zhian, J. AL-Barazanji Trends of Annual Mean Surface Air Temperature over Iraq. *Nat. Sci.* **2013**, *11*, 138–145.

76. Yang, J.; Wang, Y.Q.; Sun, Z.; Wang, Q.Q.; Batkhishig, O.; Ouyang, Z.; Cammalleri, C.; Sepulcre-Cantó, G.; Vogt, J.; Mavi, H.S. Mapping Drought Hazard Using SPI index And GIS (A Case study: Fars province, Iran). *Remote Sens. Environ.* **2017**, *7*, 1–4. [CrossRef]

77. Kogan, F.N. Global drought watch from space. *Bull. Am. Meteorol. Soc.* **1997**, *78*, 621. [CrossRef]

78. Lambin, E.F. Change detection at multiple temporal scales: Seasonal and annual variations in landscape variables. *Photogramm. Eng. Remote Sensing* **1996**, *62*, 931–938.

79. Julien, Y.; Sobrino, J.A. Comparison of cloud-reconstruction methods for time series of composite NDVI data. *Remote Sens. Environ.* **2010**, *114*, 618–625. [CrossRef]

80. Friedl, M.A.; Davis, F.W. Sources of variation in radiometric surface temperature over a tallgrass prairie. *Remote Sens. Environ.* **1994**, *48*, 1–17. [CrossRef]

81. Goward, S.N.; Xue, Y.; Czajkowski, K.P. Evaluating land surface moisture conditions from the remotely sensed temperature/vegetation index measurements: An exploration with the simplified simple biosphere model. *Remote Sens. Environ.* **2002**, *79*, 225–242. [CrossRef]

82. Gupta, R.K.; Prasad, T.S.; Vijayan, D. Estimation of roughness length and sensible heat flux from wiFS and NOAA AVHRR data. *Adv. Sp. Res.* **2002**, *29*, 33–38. [CrossRef]

83. Gaikwad, S.V.; Kale, K.V.; Kulkarni, S.B.; Varpe, A.B.; Pathare, G.N. Agricultural Drought Severity Assessment using Remotely Sensed Data: A Review. *Int. J. Adv. Remote Sens. GIS.* **2015**, *4*, 1195–1203. [CrossRef]

84. Nemani, R.R.; Running, S.W. Estimation of Regional Surface Resistance to Evapotranspiration from NDVI and Thermal-IR AVHRR Data. *J. Appl. Meteorol.* **1989**, *28*, 276–284. [CrossRef]

85. Karnieli, A.; Bayasgalan, M.; Bayarjargal, Y.; Agam, N.; Khudulmur, S.; Tucker, C.J. Comments on the use of the Vegetation Health Index over Mongolia. *Int. J. Remote Sens.* **2006**, *27*, 2017–2024. [CrossRef]

86. Al-Quraishi, A.M.F.; Sadiq, H.A.; Messina, J.P. Characterization and Modeling Surface Soil Physicochemical Properties Using Landsat Images: A Case Study in the Iraqi Kurdistan Region. *Int. Arch. Photogramm. Remote Sens. Spatial Inf. Sci.* **2019**, *XLII-2/W16*, 21–28. [CrossRef]

87. Gaznayee, H.A.A.; Al-Quraishi, A.M.F. Analysis of agricultural drought, rainfall, and crop yield relationships in Erbil province, the Kurdistan region of Iraq based on Landsat time-series MSAVI2. *J. Adv. Res. Dyn. Control Syst.* **2019**, *11*, 536–545. [CrossRef]

88. Gaznayee, H.A.A.; Al-Quraishi, A.M.F. Analysis of Agricultural Drought's Severity and Impacts in Erbil Province, the Iraqi Kurdistan Region based on Time Series NDVI and TCI Indices for 1998 through 2017. *J. Adv. Res. Dyn. Control Syst.* **2019**, *11*, 287–297. [CrossRef]